MASTER THESIS

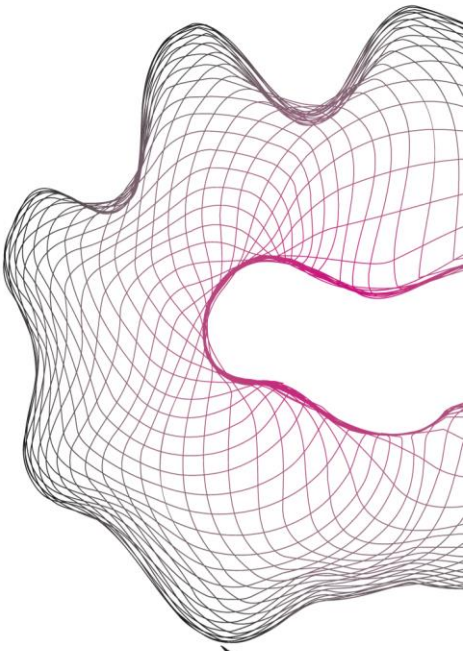

# DECODING NEURAL CONTROL STRATEGIES UNDERLYING HUMAN MOVEMENT

I. E. Gomez Orozco

FACULTY OF ENGINEERING TECHNOLOGY
DEPARTMENT OF BIOMECHANICAL ENGINEERING

**EXAMINATION COMMITTEE**
Prof. dr. ir. M. Sartori
R. E. ornelas Kobayashi, MSc
Dr. S. U. Yavuz

**DOCUMENT NUMBER**
BE - 940

UNIVERSITY OF TWENTE.

AUGUST
2023

# Contents

# Abstract

Understanding the neural mechanisms involved in the generation of human movement is fundamental for the development of technologies oriented to motor control and neurorehabilitation. One of the integral concepts for understanding motor control are α-motor neurons (MNs). MNs are excitable cells that control the activation of the skeletal muscle they innervate. Therefore, exploring the neural mechanisms underlying the activation and modulation of MNs is essential for a complete comprehension of human movement. However, the study of these neural mechanisms is constrained by the number of MNs that current approaches can observe. Therefore, in this work, we implement person-specific biophysical MN models, previously developed, that can reproduce neural firing dynamics from the entire pool of MNs. These models represent the neural excitability as a subject-specific constant gain, represented as $\Delta IF$. However, it has been reported that neural excitability changes as a function of the rate of force development (RFD). Hence, this work proposes an approach to demonstrate that $\Delta IF$ changes depending on the RFD. For this purpose, first, we examine the firing characteristics at different force levels and RFDs of *in vivo* decomposed MNs from the tibialis anterior muscle (TA) from four healthy subjects. Second, we compare the neural firing dynamics reproduced by the *in silico* models, created specifically for every subject and driven by its corresponding constant $\Delta IF$, with the neural firing dynamics observed *in vivo* at different RFDs. Finally, we propose a methodology to optimize $\Delta IF$ that best reproduces the neural firing dynamics at different RFDs, turning a person-specific $\Delta IF$ into a function of the RFD. Therefore, the objective of this study is to characterize the neural excitability, represented as $\Delta IF$ in the neural biophysical models, as a function of the RFD. This approach can create new opportunities in analyzing and understanding human movement control, enabling the development of new neuro-prosthetic devices.



***Keywords:*** *Neural excitability, motor neuron*

# Introduction

The study of human movement has multiple applications, such as the development of motor control technologies, neurorehabilitation, and sports. In a general sense, human movement is generated by a series of interactions between the nervous and musculoskeletal systems [1], where muscle contraction is responsible for generating the movement of a joint. Muscle contraction is controlled by α-motor neurons (MNs) generating action potentials [2], [3]. MNs receive multiple excitatory inputs through different descending pathways of the central nervous system (CNS) and feedback signals from afferent connections modulating their firing activity [4], [5].

Therefore, exploring the strategies utilized by the CNS to generate muscle contraction is key for the understanding of human movement. Non-invasive methods, such as decomposition algorithms, are convenient to study the neural firing activity of MNs in humans. However, these methods are constrained by the number of MNs that can be analyzed [6]. Nevertheless, recent work has demonstrated the feasibility of simulating the neural firing activity of a complete pool of MNs using person-specific biophysical neuron models [7].

In this work, we implement person-specific biophysical models to study how the excitability of the MNs firing activity changes as a function of the speed with which the force increases, also known as the rate of force development (RFD) [8].

This section provides the reader with a comprehensive introduction to relevant concepts and background information essential for understanding the project. First, important concepts such as motor control, motor units, the neural strategies underlying force modulation, and the intricate relationship between the neural drive to the muscles and force generation are introduced. Next, tools such as High-Density Electromyography (HD-EMG) and decomposition algorithms that enable the measurement of neural firing activity are discussed. Finally, procedures to simulate neural firing activity, are explored. At the end of this section, the reader is also introduced to the problem statement of this project.

## 0.1. Motor control

### 0.1.1. Motor neurons

Motor units are the fundamental unit of movement where their primary function is to convert synaptic input received by the MN into mechanical output by the muscle [9]. Motor units consists of a MN and the muscle fibers it innervates [10]. MNs are organized in pools located in the ventral horn of the spinal cord, with each pool innervating a specific muscle [11]. A MN consists of a soma, dendrites, and axon. The soma is the body of the MN where contains the nucleus of the cell and other cellular structures responsible for the correct functioning of the cell, the dendrites are branches conveying inputs to the soma, and the axon transmits the signals integrated in the soma towards the muscle fibers [12]. The MN membrane contains different ion channels, mainly including sodium $Na^+$, potassium $K^+$, and calcium $Ca^{2+}$, that are sensitive to changes to voltage in the membrane. These ion channel regulate the transition of ions between the intracellular and extracellular environments [13]. Consequently, when there is a change in the electric gradient and the membrane reaches to a specific voltage threshold, the MN generates an action potential

[14]. MN excitability or neural excitability refers to the property of MNs to generate an action potential in response to a stimulus. The neural excitability is determined by the intrinsic properties of the MN, such as the amount of different ion channels, and the size of the MN [15]. Therefore, MNs are excitable cells that modulate muscle force gene by the generation of action potentials [16].

Moreover, MNs exhibit variations in morphology and excitability according to their functionality in muscle activation [17]. The size of the MN affects the electric resistance of its membrane [18], where smaller MNs offer a larger resistance compared to bigger MNs. Therefore, by Ohm's law, where voltage is given by the product between resistance and current, when they are exposed to an excitatory current, smaller MNs are activated before larger ones [18]. This is behavior is known as the Henneman's principle [17], where it states that MNs are recruited in a size-dependent manner [19].

Studies have shown a saturation effect in the rate at which MNs generate action potentials, which can be attributed to their intrinsic excitability characteristics [20], [21]. One plausible explanation for this rate saturation is due to the presence of persistent inward currents (PICs) within the MN membrane [20]. PICs are voltage-sensitive sodium and calcium channels located in the dendrites of the MNs, acting as gain factors by amplifying and sustaining the synaptic input [22], [23]. Experimental evidence has demonstrated that PICs generate an initial amplification followed by a significant saturation when the synaptic input is transmitted through the dendrites of the MNs [22], [24].

MNs receive different information through synapses from different sources [25]. Motor commands originate mainly in the primary motor cortex, and subcortical regions of the brain [26], [27], and are transmitted through different descending pathways until converging in MNs that innervate the skeletal muscles [28]. Additionally, MNs receive motor commands from multiple layers of interneurons in the spine [29], [30], and afferent signals as a feedback system from sensory neurons in the muscle [4], [5], [31].

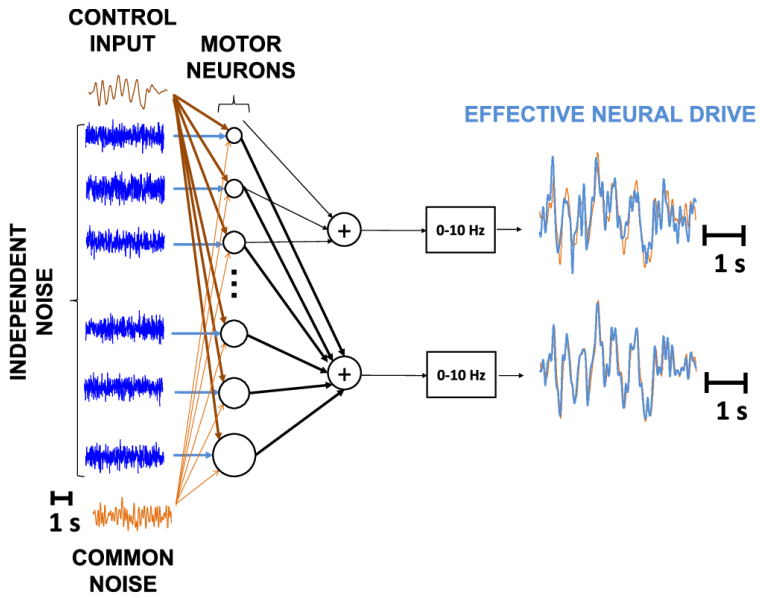


*Figure 1. The common synaptic input is the neural drive to the muscle. The MNs receive information from different sources including motor commands or control input, independent noise, and common noise. A pool of MNs acts as a low-pass filter capturing the low frequency components of the signal inputs. The output of the pool of MNs, referred as the effective neural drive to the muscle, is highly correlated to the control input. Figure obtained from [32].*

The multiple synaptic inputs received by a pool of MNs are integrated and transformed into the neural drive controlling muscle activation [33], [34]. Studies have revealed a strong correlation between the neural drive to the muscles and the force profile exerted by the muscle [32]. Therefore, the analysis of the neural drive is fundamental to estimate muscle force. The neural drive is constituted by the summation of the firing activity produced by the MNs [34]. Due to the nonlinear behavior of individual MNs [32], signal components present in the MN output may not be present in their inputs. However, the low-frequency components of a common current input shared by multiple MNs, *i.e.,* common synaptic input (CSI), will be present in the output of the set of MNs (Figure 1). Therefore, a pool of MNs can be seen as a low pass filter, where the neural drive is the linear transformation of the low-frequency components in the CSI [34]. Moreover, the larger the set of MNs analyzed receiving the CSI, the greater is the correlation with the force profile [32].

### 0.1.2. Modelling alpha-motor neurons

There are multiple methods to model the neural dynamics involved in the generation of action potentials, such as biophysical models, spiking neural models, and neuromorphic models [35], [36], [37], [38]. Biophysical models, such as the Hodgkin-Huxley model [36], where the generation of action potentials is determined by the physiological properties of the neuron (*e.g.,* ion channel dynamics, etc). In these models, motor neurons can be modeled as compartmental representations of soma and dendrite, where each compartment is represented by an electric circuit including different parameters representing the physiological properties of the neurons [35]. Figure 2 shows a neuron model representation of the soma compartment that includes a membrane capacitance ($C_s$), leakage ($g_{ls}$), sodium ($g_{Na}$), and slow ($g_{Ks}$) and fast ($g_{Kf}$) potassium channels responsible to replicate neuron firing activity. The action potentials generated by a depolarization of the membrane are described by equations ( 1 ), ( 2 ), ( 3 ), and ( 4 ).

$$C_s \frac{dV_s(t)}{dt} = -g_{ls}(V_s(t) - E_l) - I_{ion}(t) + I_{inj-s}(t) \quad (1)$$

$$I_{ion}(t) = \bar{g}_{Na} m^3 h(V_s(t) - E_{Na}) + \bar{g}_{Kf} n^4 (V_s(t) - E_K) + \bar{g}_{Ks} q^2 (V_s(t) - E_K) \quad (2)$$

$$g_{ls} = \frac{2\pi r_s l_s}{R_{m-s}} \quad (3)$$

$$C_s = 2\pi r_s l_s C_m \quad (4)$$

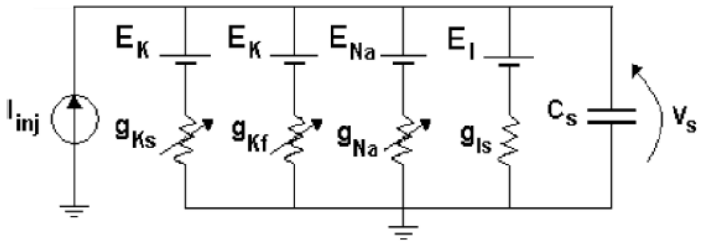


*Figure 2. Neuron model representing the soma compartment as an electric circuit. The membrane capacitance is represented as $C_s$. The model includes sodium $g_{Na}$, slow potassium $g_{Ks}$, fast potassium $g_{Kf}$ ion channels as electric conductances with their respective reverse potentials $E_{Na}$, and $E_K$. $E_l$ represents the leakage Nernst voltage and $I_{inj}$ the current injected in the soma. Figure obtained from [35].*

Where $m$ and $h$ represent the dynamics of the activation and inactivation of the sodium channel, $n$ represents the activation dynamics of the fast potassium channel, and $q$ the activation dynamics of the slow potassium channel. These state variables are voltage-dependent and their behavior is described by a set of first order differential equations involving voltage-dependent rate constants $\alpha_m, \beta_m, \alpha_h, \beta_h, \alpha_n, \beta_n, \alpha_q, \beta_q$ [13] , [35]. Solving these differential equations require small integration steps that increase the computational cost. To optimize computational efficiency, the time evolution of these rate constants can be approximated using a pulse-based model [39]. This method allows the direct estimation of the activation and inactivation variables by representing the behavior of the time course of the voltage-dependent rate constants as pulses.

### 0.1.3. Force modulation

Neural strategies underlying force control include recruitment and rate coding. Recruitment involves the systematic activation of MNs, while rate coding refers to the frequency at which the MN generates action potentials [40].

The relationship between MN pool activation (*i.e.,* number of recruited MNs within the pool) and the muscle force, normalized with the maximum voluntary contraction (MVC), generated in response is described by an exponential curve (Figure 3) [41]. The curves depicted in Figure 3 represent the MN pool activation from the tibialis anterior muscle (TA) and the first dorsal interosseous muscle (FDI). The TA and the FDI recruitment were obtained from ramp isometric voluntary contractions at low RFDs (MVC/s), 10 %MVC/s and 5% MVC/s respectively [41], [42], [43]. Due to the exponential function, recruitment coding has more influence on force generation at low force levels at the initial phase of the contraction [44]. In contrast, rate coding assumes a more prominent role in modulating force at intermediate and high force levels during isometric contractions [45].

Nevertheless, studies have demonstrated that the recruitment threshold and the firing rate of a MN are not fixed to a specific force level but is rather influenced by the RFD and the type of muscle contraction [40], [44]. For higher RFDs, MNs are recruited at lower force levels [46], [47]. This change in the neural strategies for force modulation may be caused by a modulation of neural excitability, changing the intrinsic parameters of a MN to be activated at lower force thresholds. Moreover, during ballistic contractions, when the muscle generates high forces at high speed, MNs have been observed to initially fire action potentials at very high frequencies, which then decrease over time, meaning a more substantial increase in neuron excitability [46].

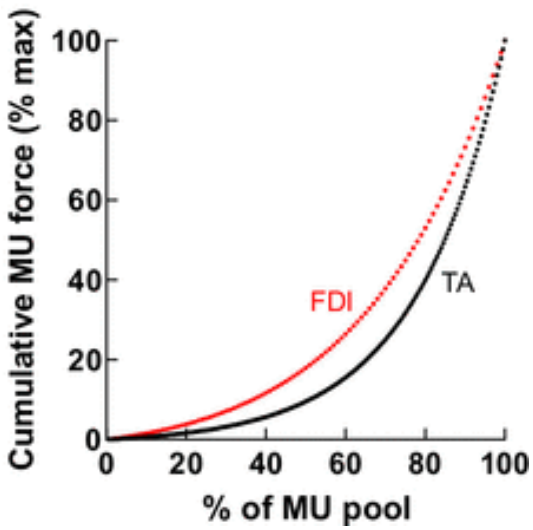


*Figure 3. Recruitment curves showing the exponential relationship between the cumulative generated force and the percentage of recruited MNs within a pool for the tibialis anterior muscle (TA) and the first dorsal interosseous muscle (FDI). These curves were obtained from ramp isometric voluntary muscle contractions at low RFDs. Figure obtained from [41].*

## 0.2. Interfacing with alpha-motoneurons

The measurement of neural activity can be accomplished through invasive or noninvasive methods. Invasive techniques involve the insertion of electrodes directly into the muscle, providing higher accuracy [48]. On the other hand, noninvasive methods rely on capturing the surface electrical signal generated by the contracting muscle [49]. Although intramuscular electrodes offer higher precision, noninvasive electrodes present several advantages. They eliminate the need for a clinically controlled environment, allow the study of sensitive muscles and capture a larger number of motor units contributing to muscle contraction [50].

Electromyography (EMG) measures the electrical activity generated by the muscles and can be used to estimate the neural activation of the muscle [49]. The EMG signal is composed of the superimposition of action potentials generated by the MNs [51]. To identify individual MN firing activity, significant advancements have been made in developing reliable multichannel blind source separation algorithms, such as Convolution Kernel Compensation (CKC) [48], [49], [52]. This method discriminates the superimposed action potentials constituting the EMG signal into individual MN firing activity in different locations of the muscle. Therefore, this method involves using monopolar electrodes arranged in a two-dimensional configuration to measure the electrical activity on the surface of the muscle from multiple locations. This system is referred to as high-density surface EMG (HD-EMG) [53]. HD-EMG measures the electrical activity across different channels creating a spatial resolution, allowing the identification of different sources.

However, it is important to note that this method presents some limitations. First, the HD-EMG restricts the identification of only a limited amount of MNs due to the number of electrodes available in its configuration. Second, the larger and superficial MNs tend to overlap smaller and deeper MNs due to the action potential surface size [49].

## 0.3. Analysis of human neuromechanics

Understanding the MN's firing dynamics and the generation of muscle force can lead to improvements in such fields as bionics, neurorehabilitation, and sports. Using interface methods, for example, the HD-EMG decomposition algorithms [48], [53], and neural models is beneficial to the study of neural firing activity. Interface methods allow the recording and study of experimental MN firing activity, while neural models estimate the firing activity of MNs in response to a stimulus. However, as mentioned in section 0.2, there are technical limitations in the current methods used to analyze experimentally the firing characteristics in MNs. Additionally, studies demonstrate that neural aspects influencing firing activity vary for every person, where factors such as age, level of training, neural injury, and motor disorders contribute to this variation [54], [55], [56], [57], [58], [59].

Therefore, recent research has proposed a methodology using HD-EMG decomposition, a single-compartment biophysical model, and optimization algorithms to create *in silico* MNs pools comprising person-specific parameters [7]. Furthermore, this methodology represents neural excitability as a gain factor, $\Delta IF$ $\left(\frac{HZ}{\eta A}\right)$, specific for every person, that linearly scales the neural drive to compute the CSI represented in the soma. Thus, the CSI represents neural signals, such as from interneurons, afferent pathways, and neuromodulatory inputs, contributing to the MN activation. Therefore, since $\Delta IF$ determines the magnitude of the CSI to generate an action potential, it reflects the neural excitability.

With this approach, it is possible to analyze the firing dynamics of complete pools of MNs, and consequently, estimate the muscle force.

## 0.4. Problem statement

The study of neural firing activity is crucial for understanding the neural strategies implemented by the CNS to control muscle activation and consequently force generation. Numerous studies have explored the relationship between MN's discharge rate and recruitment coding [60], [61], [62], [63]. Moreover, research has reported that the RFD is produced by a change in neural excitability, influencing the recruitment and rate coding strategies [47], [64], [65], [8], [66], [67]. However, as mentioned in section 0.2, there are technical limitations in the current methods used to analyze the firing characteristics in MNs. In non-invasive methods, the main limitation is due to the restricted number of MNs that can be analyzed, thus the decomposed MNs do not represent the neural behavior of the entire pool innervating a muscle.

The methodology mentioned in section 0.3 aims to address this limitation. However, this method was assessed by estimating the MN pool firing parameters with a specific RFD, 20% MVC/s, and a constant person-specific $\Delta IF$. Since the MN excitability changes, and consequently the firing pattern, depending on the RFD, the present work aims to analyze and characterize the parameter $\Delta IF$ across different RFDs using optimization algorithms and a single-compartment person-specific biophysical model comprising the entire pool of MNs innervating the TA. Thus, the goal of this research is to analyze whether by estimating $\Delta IF$ for multiple RFDs, the neural model, optimized for only 20% MVC/s, can reproduce realistic firing activity at multiple conditions.

In this way, this study contributes by estimating $\Delta IF$ as a function of the RFD for the analysis of the neural firing activity of an entire pool of MNs for multiple conditions, both for different force levels and RFDs, using non-invasive methods. Therefore, this approach contributes to the development of technologies that help people with impairments and in neurorehabilitation.

# 1. Introduction

Alpha-motor neurons (MNs) are key elements in motor control since they represent the final pathway of the nervous system and the interface with the musculoskeletal system. MNs are excitable cells that produce action potentials in response to a stimulus [16] with the excitability of the MNs modulated according to the motor task. Studies have reported a change in MN excitation when varying the rate at which muscle force is generated over time, known as the rate of force development (RFD) [46], [47], [64], [68]. Therefore, to understand the neural strategies underlying human movement, it is essential to analyze and characterize how MN excitability is modulated according to the RFD.

In this context, neural excitability is an intrinsic property of MNs determined by multiple factors such as the ionotropic and neuromodulatory systems [15], [69], [70]. The ionotropic system refers to the modulation of the opening of ion channels by neurotransmitters to depolarize the MN, while the neuromodulatory system relates to the use of neurotransmitters to alter the intracellular dynamics and change the MN's response to subsequent ionotropic inputs [69]. Additionally, the MN size is one of the parameters contributing to the excitability of the MN, since MNs with smaller sizes offer a larger electric resistance, therefore, being activated first given a current input [18].

The nervous system implements different strategies to modulate the force exerted by the muscle, such as recruitment and rate coding [71]. Recruitment coding refers to the number of MNs that are activated within the pool. According to Henneman's size principle [19], MNs are recruited in an orderly fashion based on their size, with the smallest motor neurons being recruited first and the largest motor neurons being recruited last. Rate coding represents the frequency at which these MNs are generating action potentials.

Numerous studies have explored the relationship between recruitment and rate coding, providing significant insights into the neural techniques involved in force generation and its modulation [72], [62], [73]. However, the relative contribution of these two neural strategies may vary depending on the specific muscle, the task performed, and the RFD [40], [44]. Therefore, there is a knowledge gap on how these two strategies are modified at multiple RFDs. Additionally, due to technical limitations [48], the study of MNs' firing activity is constrained to a small number of MNs that can be analyzed, thus not representing the firing behavior of the entire pool of MNs.

To address this challenge, previous work [7] has shown that *in silico* MN pools can reproduce neural firing activity and estimate the force profile during isometric contractions. This method involved optimization algorithms and person-specific biophysical models driven by a common synaptic input (CSI). The CSI represents all the synaptic signals, such as cortical, from interneurons, and afferent pathways, contributing to the activation of the MNs. The CSI was derived as the product between the neural drive to the muscle and a person-specific gain ($\Delta IF$). Therefore, $\Delta IF$ reflects the neural excitability because it determines the magnitude of the CSI. In this method, $\Delta IF$ and the parameters comprising the pool of MNs were computed by optimization algorithms, and the data obtained at 20% MVC/s RFD.

Based on the evidence, that the neural excitability changes in function of the RFD [8], [74], [75], in this work we use person-specific biophysical models of four healthy subjects to analyze and characterize $\Delta IF$ to study the adjustments in the neural excitability and the effects on the recruitment and rate coding across different RFDs.

This research demonstrates that the excitability gain $\Delta IF$ is not a constant value but rather a function of the RFD. Understanding how the nervous system modulates neural excitability across multiple RFDs, yields valuable knowledge about the neural strategies involved in the generation of force. The current study assesses the contribution and effects of neural excitability in MN firing behavior using person-specific *in silico* pools optimized for a 20% MVC/s RDF specifically. We hypothesize that by adjusting a person-specific excitability gain $\Delta IF$

according to the RFD, the *in silico* MN pool can reproduce the neural firing activity observed experimentally. As a result, the MN pool models can be driven by a person-specific $\Delta IF$ function that depends on the RFD.

The findings of this study contribute to the development of technologies in neurorehabilitation, and assistance for impaired persons, such as neuro-prosthetic devices and exoskeletons, by using non-invasive methods to model the entire pool of MNs innervating a muscle for multiple conditions. Furthermore, the obtained results offer crucial insights into how neural excitability is modulated across multiple RFDs.

# 2. Methods

## 2.1. Experimental protocol

Four healthy subjects (age: 27.4 ± 2.07 years, weight: 70 ± 12.34 kg, height: 173.6 ± 10.06 cm) participated in this study [7]. The subjects were instructed to perform isometric ankle dorsiflexion contractions at five different force levels (10%, 20%, 30%, 40%, and 50%) relative to the maximum voluntary contraction force (MVC). For each target, four rates-of-force (5%, 10%, 15%, and 20% MVC/s) were performed. A total of five repetitions for each condition. The subjects were provided with a visual reference on a screen to track the exerted force using ramp-and-hold patterns.

The HD-EMG data was recorded from the TA muscle by an 8 × 8 electrode grid and a TMSi Refa multichannel amplifier (TMS International B. V., Oldenzaal, The Netherlands) at a sampling frequency of 2048 Hz. The associated torque was recorded using a Biodex chair (M4 Biodex Medical Systems Inc., Shirley, NY, USA) and a National Instruments Data Acquisition card (NI DAQ) at a sampling frequency of 512 Hz. Both measurements were performed simultaneously.

## 2.2. In silico motor neuron pool generation

The data obtained from the HD-EMG was decomposed by a convolution kernel compensation blind source separation algorithm [48], [49], [52] to identify individual spike trains produced by the *in vivo* MNs. Subsequently, the quality of the identified MNs was assessed by a quality control algorithm rejecting non-physiologically realistic MNs according to a pulse-to-noise ratio (PNR) > 20 dB, a coefficient of variation (CoV) < 0.3, and discharge rates < 30 Hz [7], [76].

The data obtained from the 20% MVC/s RFD was used to generate *in* silico MNs copies that can reproduce the firing activity of the *in* vivo MNs [7]. This specific RFD was selected to have a wider range of MNs recruited during the different trials. For each *in vivo* decomposed MN, a CSI-driven single-compartment biophysical model was implemented to create an *in silico* MN copy [35]. The model represents the soma membrane of the MN as an electric circuit, it comprises a membrane capacitance $(C)$, leakage $(g_l)$, slow potassium $(g_{Ks})$, fast potassium $(g_{Kf})$, and sodium $(g_{Na})$ conductances responsible for the generation of action potentials. The model solves the Hodgkin and Huxley differential equations [36] using a pulse-based model method [39], where the voltage-dependent state variables $(m, h, n, q)$ that control the activation and inactivation of the different ionic channels are described by $\alpha_i$ and $\beta_i$ representing the state variables behavior as rectangular pulses, where $i$ represents each state variable. Therefore, the time evolution of the activation and inactivation dynamics of the included ion channels are represented by $\alpha_i$ and $\beta_i$. The diameter of the somma $(D_s)$, used to customize the leakage conductance and MN capacitance, represents the anatomical size of the MN.

The CSI driving the biophysical model was obtained by the linear transformation between the neural drive and a person-specific $\Delta IF_{20}$ gain, where the subscript denotes that this gain was calculated for the 20% MVC\s RFD. The neural drive was derived from the *in vivo* cumulative spike trains and $\Delta IF_{20}$ was computed using a multi-

objective optimization that minimized the recruitment error in two conditions [7]. First, the earliest recruited *in* vivo MN with the smallest *in silico* $D_s$ and, second, the latest recruited *in vivo* MN with the biggest *in silico* $D_s$.

Optimizing subject-specific the ionic channels parameters of the slow potassium activation dynamics represented as $\alpha_Q$ and $\beta_Q$ values during the pulse, and the diameter of the soma $D_s$ from the neural model, enabled the production of *in silico* MN copies that generate spikes corresponding to the *in vivo* firing activity characteristics. Furthermore, based on the distribution of these parameters from the identified *in silico* MNs, a set comprising 200 *in silico* MNs was generated for each subject to simulate a complete pool of MNs innervating the TA.

## 2.3. In vivo analysis

The *in vivo* data analysis examined the recruitment and rate coding strategies across different RFDs. The mean discharge rate during the plateau of each recorded *in vivo* MN was calculated according to ( 5 ).

$$\bar{f} = \frac{\sum\left(\frac{1}{t_n - t_{n-1}}\right)}{N} \quad (5)$$

Where $t_n$ represents the time at which the spike was observed, and $N$ refers to the total number of inter-spike lapses generated by the MN.

The MN recruitment threshold was determined as the %MVC at which a MN produced its first spike.

To compensate for the neuromechanical delay produced by a lag between the neural drive to the muscle and the force generation [77], the neural drive and the torque profile were synchronized estimating the cross-correlation function, where the peak value of the function represents the delay between the two data.

Test 1 consisted of analyzing how the discharge rate observed *in vivo* is modulated through multiple RFDs at different force levels from the four subjects by computing the mean discharge rate at 5, 10, 15, and 20% MVC/s during the plateau portion of the ramp.

## 2.4. In silico analysis

### 2.4.1. Firing dynamics

Test 2 assessed the capability of the *in silico* MN pools to reproduce *in vivo* MN firing behavior across different RFDs using a person-specific $\Delta IF_{20}$ gain corresponding to 20% MVC/s RFD (for which the *in silico* MN pool was created (section 2.2)) [7]. Therefore, test 2 examines the MN firing activity regarding recruitment and rate coding.

For each condition, force level and RFD, the repetition containing the largest number of identified MNs was selected in the present study.

To generate *in silico* MNs spikes, the CSI was used to drive the created MN models. The CSI was derived as the product between the excitability gain $\Delta IF$ and the neural drive derived from the *in vivo* generated spikes. Then, an activation function was implemented to determine the number of motor neurons that are activated. This function is based on the relationship between the recruitment properties of the TA and the force exerted by the muscle [41]. Subsequently, the generated *in silico* spikes were used to compute the mean discharge rate, and the recruitment threshold implementing the same methodology as described previously using the *in vivo* data.

To examine the performance of the current model driven by $\Delta IF_{20}$ at different RFDs, three different methods were implemented. Additionally, these methods were compared to determine the optimal function that measures the error considering the computational cost, complexity, and representation of the data.

#### *2.4.1.1. Linear model*

The first method consisted in fitting the data with a linear model describing the recruitment and rate coding. Then, the relative error between *in vivo* and *in silico* neural activity was computed as the difference between the slopes and the *y*-intercepts. Additionally, a third cost function is required in this method to describe the distribution of the data, such

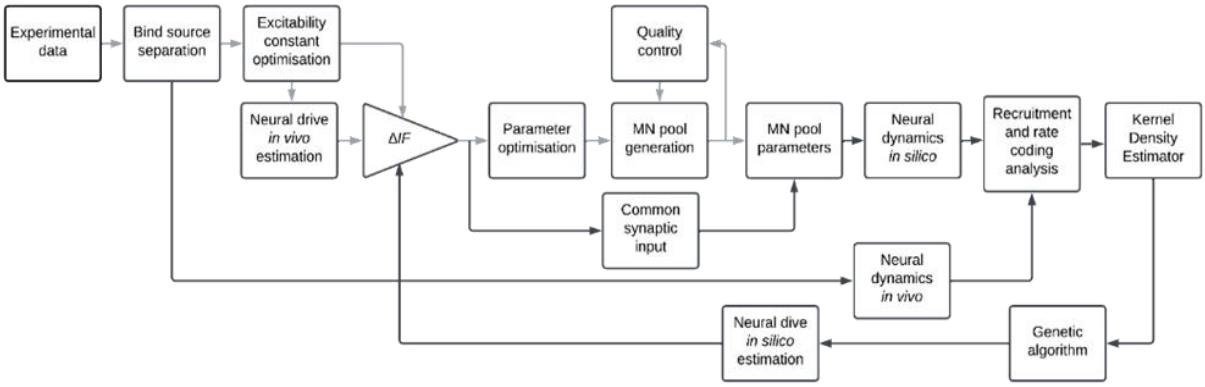


*Figure 4. Block diagram describing the process to compute ΔIF for multiple RFDs. The grey lines represent the procedures to compute a person-specific $\Delta IF_{20}$ for a specific rate of force development [7]. The black lines represent the methodology to compute a person-specific ΔIF as a function of the RFD. The experimental data is obtained using HD-EMG and convolution kernel blind source separation decomposition [52]. Subsequently, a person-specific $\Delta IF_{20}$ was estimated using optimization algorithms. The CSI was computed as the linear transformation between $\Delta IF_{20}$ and the neural drive. The MNs model is driven by the computed CSI, where the parameters were estimated by optimization algorithms to match the recruitment and firing patterns. Based on the distribution of these parameters, an entire pool comprising 200 MNs was created. Then, the entire pool, optimized with data of 20 %MVC/s, was used to produce MN firing patterns using data obtained at multiple RFDs. Finally, ΔIF was estimated by an optimization algorithm minimizing the error between the recruitment and mean firing rate using a kernel density estimator as a cost function.*

as the range of the data, consequently increasing the complexity of the model.

#### *2.4.1.2. Covariance matrix-based ellipses*

The second method involved the generation of ellipses using the covariance matrix of the recruitment and rate coding to capture the neural behavior according to (6).

$$\begin{bmatrix} x(n) \\ y(n) \end{bmatrix} = \begin{bmatrix} v_{1,x} & v_{2,x} \\ v_{1,y} & v_{2,y} \end{bmatrix} \begin{bmatrix} \sqrt{\lambda_1} & \\ & \sqrt{\lambda_2} \end{bmatrix} \begin{bmatrix} cos(n) \\ sin(n) \end{bmatrix} + \begin{bmatrix} \frac{range_1}{2} \\ \frac{range_2}{2} \end{bmatrix}_{n=0 \dots 2\pi} \quad (6)$$

Where $v$ are the eigenvectors and $\lambda$ are the eigenvalues respectively from the covariance matrix. The center of the ellipse is defined by half of the range of the recruitment and rate coding data.

Thus, the area of the *in vivo* neural activity ellipse that is not captured by the *in silico* MNs ellipse indicates the error of the *in silico* MN pool to reproduce *in vivo* firing patterns.

#### *2.4.1.3. Kernel density function*

The third method consisted in computing the probability density function from the recruitment and rate coding using a bivariate kernel density estimator, where the bandwidth was estimated as described in [78]. This method uses an asymptotic mean integrated squared error (AMISE) approach to minimize the distance between kernel density estimator and the probability density function. The relative error between the two MN sets was calculated as the previous method, calculating the excluding area of the *in vivo* MN behavior.

### 2.4.2. Force profile correlation

Test 3 measured the correlation between the neural drive and the force profile for the multiple force levels to examine the ability of the neural models driven by $\Delta IF_{20}$ to estimate the force profile across the different RFDs. The correlation between these two variables, neural drive and force profile, was measured by the coefficient of determination ($R^2$)

*Table I. Mean discharge rate (Hz) in the four subjects during the plateau portion of the contraction at the multiple RFDs and multiple force levels.*

| Force Level (%MVC) | Rate of force development (%MVC/s) | | | |
|---|---|---|---|---|
| | **5** | **10** | **15** | **20** |
| **10** | 10.76±1.5 | 10.75±1.48 | 11±1.80 | 10.76±1.44 |
| **20** | 13.04±1.48 | 12.47±1.62 | 12.17±2.34 | 13.08±1.81 |
| **30** | 13.25±1.64 | 12.61±2.55 | 13.27±1.89 | 12.05±0.96 |
| **40** | 15.06±1.80 | 14.40±1.63 | 14.29±1.63 | 14.46±1.71 |
| **50** | 16.89±1.61 | 15.17±1.14 | 13.50±2.58 | 15.31±1.85 |

*Table II. Firing activity relative error (mean±std) in vivo vs in silico estimated by the linear model method.*

| Error (%) | Rate of force development (% MVC/s) | | | |
|---|---|---|---|---|
| | **20** | **15** | **10** | **5** |
| **Slope Error** | 68.87 ± 37.14 | 381.25 ± 564.42 | 308.52 ± 252.92 | 1594.9 ± 2890.9 |
| **Intercept Error** | 24.65 ± 12.50 | 28.27 ± 20.37 | 26.52 ± 20.30 | 29.77 ± 11.67 |
| **Spread Error** | 3.60 ± 3.67 | 8.5 ± 9.12 | 22.25 ± 4.58 | 30.87 ± 14.14 |

obtained by computing a linear regression model for every subject.

### 2.5. $\Delta IF$ Optimization

Figure 4 describes the process followed in this study for the estimation of a person-specific excitability gain $\Delta IF$as a function of the RFD.

Test 4 consisted of computing a person-specific $\Delta IF$ gain for each RFD that best describes the *in vivo* neural dynamics was performed by implementing a genetic optimization algorithm in MATLAB (The MathWorks, Inc., Natick, MA, USA). The optimization algorithm minimized the relative error of the excluding *in vivo* neural activity area derived by the kernel density estimator method.

The optimization algorithm was initiated with a population size of 70, an elite percentage of 10%, a cross-over of 70% using a heuristic function according to ( 7 ), a mutation rate of 5%, and a function tolerance of 0.01. These parameters were chosen to minimize the computation time.

$$child = parent_2 + ratio * (parent_1 - parent_2) \quad (7)$$

The optimized $\Delta IF$ excitability gains obtained for the four subjects were used to drive the *in silico* MN pools to generate simulated spikes at their corresponding RFD. Subsequently, the neural firing dynamics were examined and compared with the analysis performed in section 2.4.1.

## 3. Results

### 3.1. Rate coding analysis

Figure 5 shows the rate coding analysis *in vivo* for multiple RFDs and force levels. A linear model was implemented to compare the discharge rates obtained from the four subjects. The mean discharge rate (Hz) for all the subjects at 5, 10, 15, and 20% MVC/s for the multiple force levels is presented in Table I.

### 3.2. Neural firing dynamics

The three proposed methods were tested to analyze their performance to estimate the error at different RFDs between *in vivo* identified MNs and *in silico* generated MN pool models driven by $\Delta IF_{20}$. Figure 5 shows an example from subject 4 of the linear model method. This method measured the relative error in the slope of the model, the intercept, and the spread or distribution of the data. The mean errors between the four subjects using the linear method model are presented in Table II, where the error of the slope and the spread decreases when increasing the RFD.

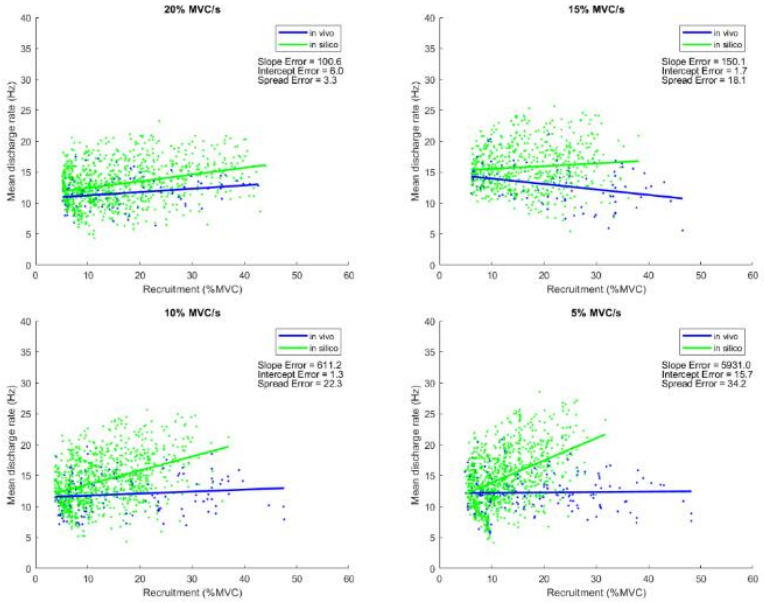


*Figure 5. Example of the relative error estimation of the firing activity at multiple RFDs (5, 10, 15, and 20% MVC/s) between in vivo MNs (blue) vs in silico generated MN models (green) driven by $\Delta IF_{20}$ using the linear model method (subject 4). With this method three cost functions are estimated: Slope error, intercept error, and spread error*

*Table III. Firing activity relative error (mean±std) in vivo vs in silico estimated by the covariance matrix-based ellipse method.*

| | Rate of force development (%MVC/s) | | | |
|---|---|---|---|---|
| | **20** | **15** | **10** | **5** |
| **Error (%)** | 10.02 ± 6.75 | 30.47 ± 21.48 | 36.7250 ± 7.28 | 45.40 ± 12.65 |

*Table IV. Firing activity relative error (mean±std) in vivo vs in silico estimated by the bivariate kernel density function method.*

| | Rate of force development (%MVC/s) | | | |
|---|---|---|---|---|
| | **20** | **15** | **10** | **5** |
| **Error (%)** | 0.67 ± 0.47 | 7.92 ± 9.18 | 10.50 ± 5.62 | 23.62 ± 14.20 |

A representation of the covariance matrix-based ellipse method for subject four is shown in Figure 6, where the relative error is estimated as the excluding area of the ellipse that captures the in vivo neural dynamics. The mean errors from the four subjects across the different RFDs are shown in Table III.

Lastly, an example from subject four of the kernel density function method is illustrated in Figure 7. Additionally, Table IV summarizes the relative errors for the four subjects across the multiple RFDs. These errors were estimated by the relative difference between the areas computed by the kernel density functions. The upper recruitment threshold of the *in silico* models decreases from ~50% MVC to ~32% MVC when decreasing the RFD from 20% MVC/s to 5% MVC/s respectively.

Figure 8 shows the estimated relative error for the four subjects using the kernel density function between *in vivo* and *in silico* generated spikes. The error (mean±std) of the four subjects yielded the following results: 0.66%±0.48 at 20% MVC/s, 7.91%±9.18 at 15% MVC/s, 10.50%±5.66 at 10% MVC/s, and 23.60%±14.21 at 5% MVC/s.

## 3.3. Neural drive and force correlation

The correlation analysis between the force profile and the computed neural drive from the *in vivo* identified MNs and *in silico* MN models, driven by $\Delta IF_{20}$, for the four subjects throughout the different conditions, force levels and RFDs, is shown in Figure 9. The mean coefficient of determination of the *in* vivo MNs of all subjects yield the following values: $R^2 = 0.90 \pm 0.03$ for 5% MVC/s, $R^2 =$

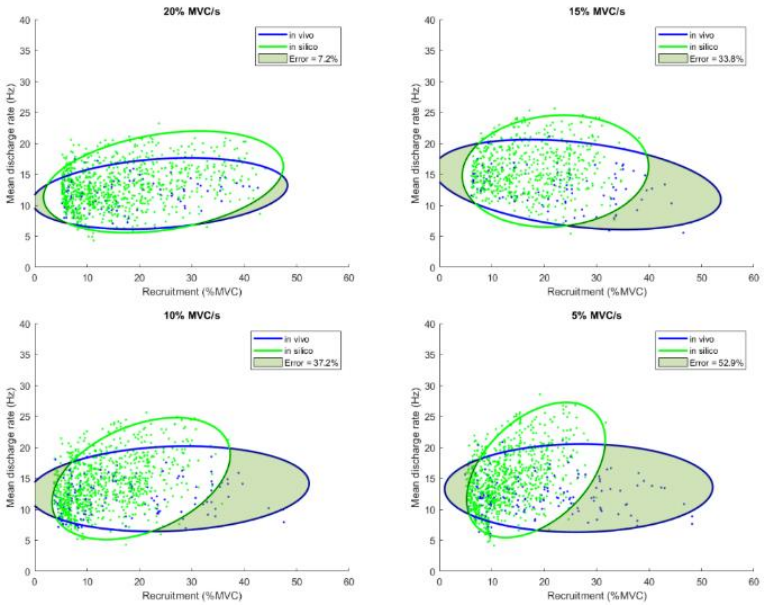


*Figure 6. Example of the relative error estimation of the firing activity at multiple RFDs (5, 10, 15, and 20% MVC/s) between in vivo MNs (blue) vs in silico generated MN models (green) driven by $\Delta IF_{20}$ using the covariance matrix-based ellipse method (subject 4). This method estimates only one cost function: the difference between the areas of the computed ellipses.*

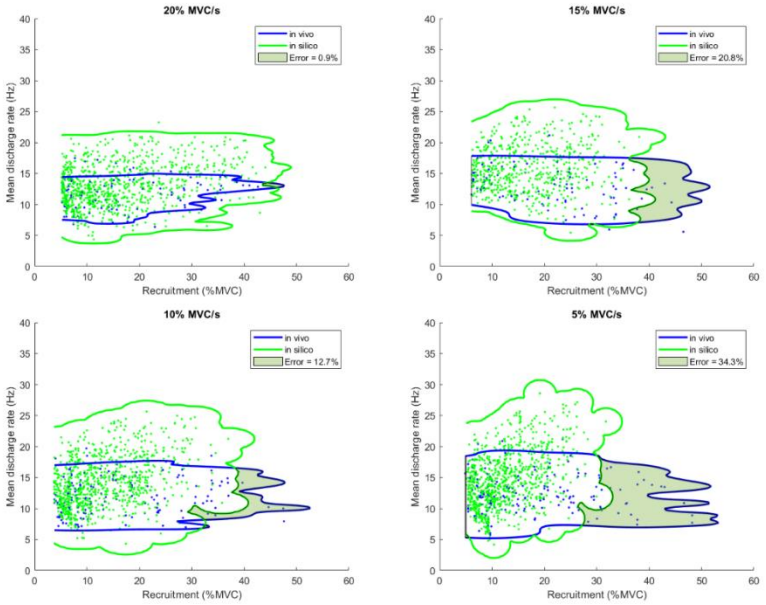


*Figure 7. Example of the relative error estimation of the firing activity at multiple RFDs (5, 10, 15, and 20% MVC/s) between in vivo MNs (blue) vs in silico generated MN models (green) driven by $\Delta IF_{20}$ using the kernel density function method (subject 4). This method estimates only one cost function: the difference between the areas of the kernel density functions.*

$0.92 \pm 0.02$ for 10% MVC/s, $R^2 = 0.91 \pm 0.05$ for 15% MVC/s, and $R^2 = 0.91 \pm 0.05$ for 20% MVC/s.

### 3.4. $\Delta IF$ Optimization

After the optimization of $\Delta IF$ across multiple RFDs using the kernel density function method, a person-specific excitability function $\Delta IF$ that best minimizes the error between *in vivo* and *in silico* neural data was computed. The optimization time required to find the optimal $\Delta IF$ was ~50 hours/RFD using a parallel computation with 12 workers, 128GB of RAM, and an AMD Ryzen

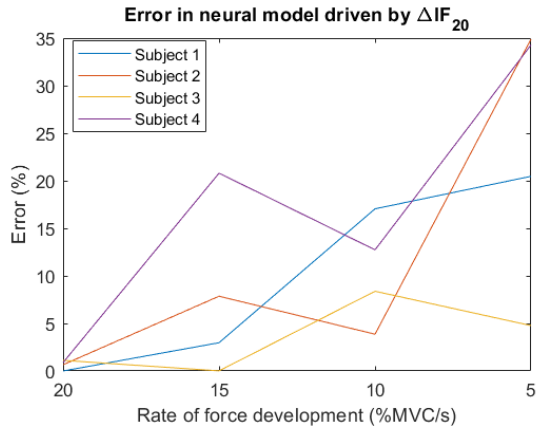


*Figure 8. Relative error between in vivo and in silico generated neural firing activity driven by $\Delta IF_{20}$ across multiple RFDs for the four subjects. The error was estimated using a bivariate kernel density estimator to compute the difference in the distributions of the recruitment and rate coding. For the four subjects the error increases when decreasing the RFD.*

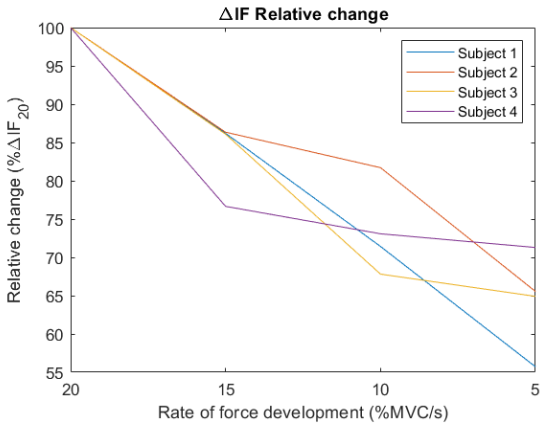


*Figure 10. Subject-specific excitability gain $\Delta IF$ as a function of the RFD. $\Delta IF$ was computed using optimization algorithms minimizing the error between the in vivo and in silico firing activity using a bivariate kernel estimator. This figure represents the relative change of $\Delta IF$ with $\Delta IF_{20}$. For the four subjects $\Delta IF$ decreases when decreasing the RFD.*

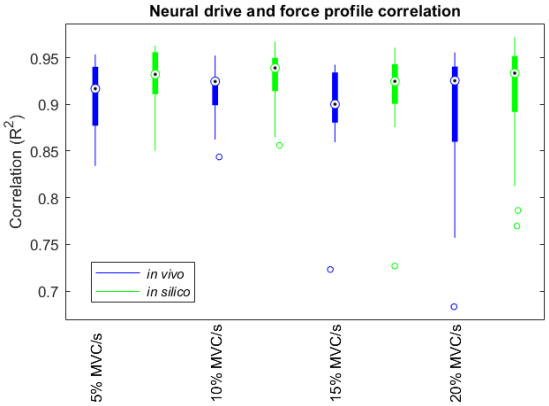


*Figure 9. Correlation analysis of the force profile and the neural drive for in vivo MNs (blue) and in silico generated models (green) driven by $\Delta IF_{20}$. The correlation analysis was performed estimating the coefficient of determination $(R^2)$using a regression model between the neural drive and the force profile.*

Ryzen Threadripper 3990X 64-Core processor 2.90 GHz.

The relative change of the inter-subject excitability gain $\Delta IF$values compared to $\Delta IF_{20}$ across all the studied RFDs is presented in Figure 10. As can be observed, the neural excitability gain $\Delta IF$ decreases when decreasing the RFD for all the subjects up to ~45% relative to $\Delta IF_{20}$. Additionally, the specific

*Table V. Subject-specific excitability values $\Delta IF$ $\left(\frac{Hz}{\eta A}\right)$ at each RFD analyzed.*

| Subject (#) | Rate of force development (%MVC/s) | | | |
|---|---|---|---|---|
| | **20** | **15** | **10** | **5** |
| **1** | 0.4889 | 0.4214 | 0.34918 | 0.2724 |
| **2** | 0.4467 | 0.3857 | 0.3650 | 0.2928 |
| **3** | 0.4477 | 0.3854 | 0.3063 | 0.2906 |
| **4** | 0.5613 | 0.4303 | 0.4102 | 0.4001 |

$\Delta IF$ values obtained after the optimization procedure are presented in Table V for every subject.

Figure 11 shows an example from subject four comparing the firing activity captured by the bivariate kernel estimator between *in vivo* and *in silico* MNs driven by the optimized function $\Delta IF$. As it can be seen, the *in silico* MN models driven by the optimized $\Delta IF$ present a better performance in tracking the *in vivo* neural activity reducing the error.

The error (mean$\pm$std) for the four subjects, estimated by the kernel density function method of the firing dynamics using *in silico* MN pool driven

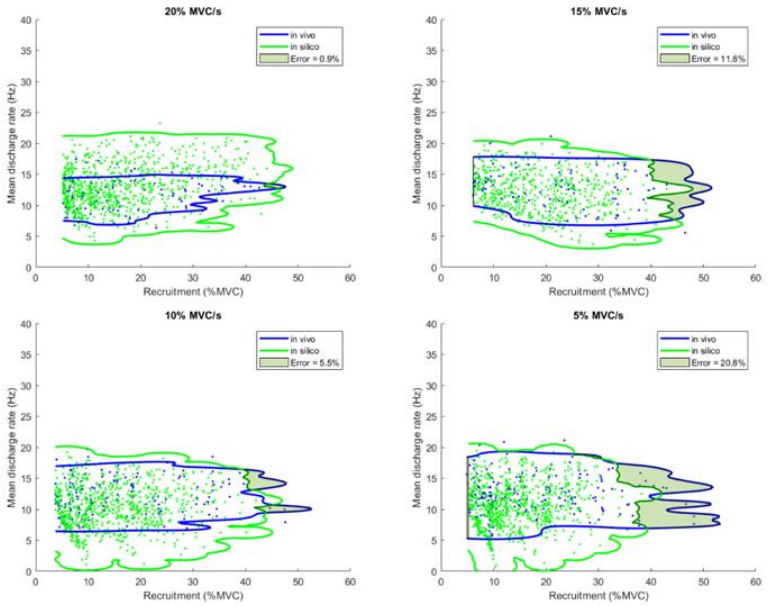


*Figure 11. Example of the relative error estimation of the firing activity at multiple RFDs (5, 10, 15, and 20% MVC/s) between in vivo MNs (blue) vs in silico generated MN models (green) driven by $\Delta IF$ optimized for the multiple RFDs using the kernel density function method (subject 4). The optimized $\Delta IF$ increases the recruitment threshold at low RFDs reducing the estimated error.*

*Table VI. Firing activity relative error (mean±std) in vivo vs in silico estimated by the bivariate kernel density function method after optimization of $\Delta IF$.*

| | **Rate of force development (%MVC/s)** | | |
|---|---|---|---|
| | **15** | **10** | **5** |
| **Error (%)** | 4.54±5.30 | 6.30±3.83 | 14.03±8.51 |

*Table VII. I*mprovement in *reproducing* in vivo neural *firing* activity using in silico MN models driven by $\Delta IF$ optimized as a function of the RFD *relative to* in silico MN models driven by $\Delta IF_{20}$.

| **Subject (#)** | **Rate of force development (%MVC/s)** | | |
|---|---|---|---|
| | **15** | **10** | **5** |
| **1** | 60% | 30.58% | 5.85% |
| **2** | 34.18% | 23.08% | 59.89% |
| **3** | 0% | 42.85% | 58.33% |
| **4** | 43.25% | 56.69% | 39.35% |

by the optimized $\Delta IF$ for the specific RFD, are presented in Table VI.

Additionally, the level of improvement to reproduce *in vivo* neural firing activity using *in silico* MN models driven by $\Delta IF$ relative to *in silico* MN models driven by $\Delta IF_{20}$ is presented in Table VII.

Overall, the improvement using $\Delta IF$ optimized as a function of RFD for the four subjects is 37.83%±6.44. The error is reduced for the four subjects to 34.35%±25.27 for the 15% MVC/s RFD, 38.30%±14.72 for the 10% MVC/s, and 40.85%±25.13 for the 5% MVC/s.

# 4. Discussion

## 4.1. General discussion

In this study, the neural firing activity of the TA from four healthy subjects was analyzed at different force level amplitudes (10, 20, 30, 40, and 50% MVC) and RFDs (5, 10, 15, 20% MVC/s). Person-specific biophysical neuronal models were created from the data *in vivo* obtained at 20% MVC/s. Additionally, a complete pool comprising 200 *in silico* MNs was created from the statistical properties of the model parameters [7]. Therefore, the MN pool model parameters, including the excitability gain $\Delta IF$, were optimized to reproduce

realistic firing patterns at a specific RFD (20% MVC/s).

In the current study, it has been demonstrated that neural excitability is modulated as a function of the RFD as it has been described in previous studies [46], [47], [64], [68], and consequently, the *in silico* MN pool can be driven by a CSI using the optimized $\Delta IF$ function to reproduce *in vivo* neural firing patterns. Additionally, the *in silico* MN pools can be used to estimate the force profile exerted by the muscle at the multiple ranges of the RFD regardless the $\Delta IF$ used to drive the models.

The rate coding from the observed data *in vivo* at multiple force levels and RFDs was analyzed. However, in this study, the firing activity of each individual MN was not tracked along the multiple conditions, force level and RFD. Table I shows the mean discharge rate of the four subjects during the plateau portion of the ramp contraction profile. The results indicate that overall, the recorded MNs generate action potentials at similar frequencies regardless of the RFD (5, 10, 15, and 20% MVC/s). These findings are consistent with previous research [41], [79], [80], where an increment in discharge rate is produced when increasing the force level. These results highlight the contribution of rate coding gradually increasing the fire frequency when increasing the muscle force [44]. Additionally, a previous study [81], measured MN firing activity of the first dorsal interosseus (FDI) at slow (10% MVC/s), fast (20% MVC/s) and ballistic contractions using wire electrodes. The study reported a similar discharge rate between slow and fast contractions with a substantial increment at ballistic contractions. Therefore, these findings corroborate the results of the current study.

Additionally, since the analysis of the discharge rates *in vivo* shows comparable results across the multiple RFDs, the neural drive and consequently, the CSI, contain similar amplitudes across the RFDs. *In silico* MNs are optimized to generate a spike when a voltage threshold is reached due to an input current (CSI). However, the neural firing dynamics analysis shows that *in silico* MN pool driven by the constant $\Delta IF_{20}$ cannot reproduce the neural firing dynamics observed *in vivo* at multiple RFDs, apart from the 20% MVC/s RFD, despite the excitatory input current exhibiting similarities for the multiple RFDs. These findings can be attributed to the fact that *in silico* MN pools, along with $\Delta IF_{20}$, were optimized using the data obtained at 20% MVC/s in previous work [7]. This causes that the MN pool models driven by $\Delta IF_{20}$ at 5, 10, and 15% MVC/s RFDs produce an earlier MN recruitment. This happens because the amount of electric current over time required to activate an *in silico* MN during the 20% MVC/s RFD is achieved at larger forces compared to lower RFDs due to the higher slope in force produced over time during the linear increment portion of the contraction. Consequently, *in silico* MNs at low RFDs achieve the same amount of electric current over time, for which they were optimized to be activated, at lower forces decreasing the recruitment threshold. Therefore, the optimization of $\Delta IF$ according to the RFD is essential since it scales the CSI adjusting the recruitment thresholds.

As can be observed in Figure 8, the error in neuron firing activity increases when decreasing the RFD for all subjects. However, subjects 1 and 3 present a smaller error throughout the different RFDs compared to the rest of the subjects. The MN pools of these two subjects consist mainly (>70%) of MNs generated from the statistical distribution of the *in silico* identified MNs parameters that reproduce the firing activity of *in vivo* observed MNs [7]. Therefore, since identified *in silico* MNs possess more reliable firing parameters than the generated MNs, we would expect a smaller error from the MN pools comprising a higher amount of *in silico* identified MNs.

A plausible explanation for these findings may be that the more *in silico* MNs optimized with the firing patterns observed *in vivo* at 20% MVC/s, the *in silico* pool will better represent that specific RFD. On the other hand, if most of the pool is constituted by generated MNs based on the distribution of the parameters from the identified *in silico* MNs, the pool may capture the firing parameters of another MNs that were not observed *in vivo*. Consequently, the error is larger at low RFDs for the subjects with a higher number of *in silico* optimized MNs.

As previously reported [34], [32], the correlation analysis showed a high correlation between the torque profile and the neural drive. This test measured this correlation using *in vivo* identified MNs and *in silico* generated MN models driven by $\Delta IF_{20}$ to generate the neural drive at multiple RFDs. The results indicate that there is no significant change in correlation when using the *in silico* MN-generated pool to estimate the exerted torque profile across the RFDs. These findings are unexpected since the *in silico* MN-generated models were optimized at 20% MVC/s and driven by $\Delta IF_{20}$. Therefore, we hypothesized a higher correlation at higher RFDs compared with lower RFDs since the firing dynamics change at different RFDs. This can be explained since the coefficient of determination $R^2$ is already large using the neural drive derived from *in vivo* MN. Consequently, since the neural drive is determined by the CSI [34], and therefore, the *in silico* MN models are driven by the CSI derived from *in vivo* MNs, the correlation between the neural drive and the torque profile is the same for *in vivo* and *in silico* MNs.

The cost functions test showed that the optimal method to estimate the neural firing dynamics error between *in vivo* observed MNs and *in silico* MN generated pools is the kernel density function. This method can accurately estimate the neural firing activity area (Table IV) compared to the covariance matrix-based ellipse method (Table III), where the error is over-estimated since this function assumes that the data is normally distributed and creating symmetric ellipses [82]. Additionally, the covariance matrix-based ellipse method is sensitive to extreme values since the center of the ellipse is defined by the range of the data. Furthermore, the kernel density method can capture the distribution of the data within one cost function, decreasing the computational cost compared to the linear model method (Table II) that requires three cost functions to optimize $\Delta IF$. Moreover, since the *in silico* MN generated pools contain more MNs compared to the observed *in vivo*, it modifies the trend of the data, causing the linear model to consider these additional MNs as errors increasing the cost function value.

The findings obtained from the optimization of a person-specific excitability gain $\Delta IF$ for the multiple RFDs indicate that $\Delta IF$ is modulated as a function of the RFD. Figure 10 shows that for every subject, $\Delta IF$ decreases when decreasing the RFD, indicating that neural excitability increases substantially when the muscle is contracted at high RFDs (20% MVC/s) compared to the other RFDs analyzed as suggested previously [8], [46], [47], [64], [68].

Additionally, the analysis using *in silico* MN pools driven by a person-specific $\Delta IF$ adjusted according to the RFD demonstrates an improvement to track the neural firing activity observed *in vivo*.

## 4.2. Limitations and future scope

The present study has researched how the neural excitability, modeled as $\Delta IF$ using *in silico* MN-generated models, is modified as a function of the RFD to reproduce neural activity. However, there are features and open questions for further research.

First, the estimated error between *in vivo* and *in silico* MN firing activity was minimized across the multiple RFDs analyzed in this study. However, at lower RFDs the error remains relatively high (14.03%$\pm$8.51). This can be due to the oversimplification of the neural dynamics used in this study. Therefore, future research should focus on new strategies to minimize this error by examining and integrating other parameters regarding MN excitability in the neural model [8], [35]. These strategies may include the input of different electric current amplitudes depending on the size of the MN. Thus, modulating the excitability in individual MNs. Other strategies should examine and integrate other parameters regarding MN excitability in the neural model, such as the metabotropic system and persistent inward currents of sodium and calcium. Studies have reported that the metabotropic system contributes greatly to the regulation of neural excitability at the intracellular level [69]. Additionally, persistent inward currents of sodium and calcium have a crucial impact in MN excitability since they contribute to the amplification of the synaptic current and produce a self-sustained firing activity

due to a short pulse of excitatory input [8], [69], [83], [84].

Second, the *in silico* MN models used in this study do not generate a significant change in force profile estimation across the different RFDs. Therefore, future research should investigate and link the neural firing activity of the *in vivo* and *in silico* MNs to their twitch force to correctly estimate the torque exerted by the muscle [85], [86], [87].

Third, the activation function to generate spike trains using *in silico* MN models was implemented as an exponential function [41]. However, this function is not fixed, but rather it is affected by the RFD since the recruitment threshold is shifted accordingly [46], [47], [64]. Thus, using a fixed activation function to generate *in silico* spike trains may result in inaccurate firing patterns. Therefore, future studies may examine how the activation function can be optimized, along with the *in silico* MN-generated models, for the accurate tracking of the recruitment coding for different RFDs.

Finally, the methodology implemented in this study can be examined with *in silico* MN-generated models optimized at a different RFD to compare the performance of $\Delta IF$ to reproduce neural activity. Additionally, this methodology can be implemented by exploring the neural activity of other muscles.

## 5. Conclusion

This study characterized a person-specific neural excitability gain $\Delta IF$ that drives MN pool models across multiple RFDs. The findings of this study suggest that a dynamic adjustment of $\Delta IF$ according to the RFD could generate realistic neuron firing activity using MN pool models that were optimized at a constant specific RFD.

## References


[1] J. M. Winters and S. L. Woo, Multiple muscle systems: biomechanics and movement organization, Springer Science & Business Media, 2012.

[2] V. Brezina, I. V. Orekhova and K. R. Weiss, "The neuromuscular transform: the dynamic, nonlinear link between motor neuron firing patterns and muscle contraction in rhythmic behaviors," *Journal of neurophysiology,* vol. 83, no. 1, pp. 207-231, 2000.

[3] A. Friese, J. A. Kaltschmidt, D. R. Ladle, M. Sigrist, T. M. Jessell and S. Arber, "Gamma and alpha motor neurons distinguished by expression of transcription factor Err3," *Proceedings of the National Academy of Sciences,* vol. 106, no. 32, pp. 13588-13593, 2009.

[4] F. Ranieri and V. Di Lazzaro, "The role of motor neuron drive in muscle fatigue," *Neuromuscular Disorders,* vol. 22, pp. S157-S161, 2012.

[5] J. B. Nielsen, " Human spinal motor control," *Annual review of neuroscience,* vol. 39, pp. 81-101, 2016.

[6] D. Farina, R. Merletti and R. M. Enoka, "The extraction of neural strategies from the surface EMG: an update," *Journal of Applied Physiology,* vol. 117, no. 11, pp. 1215-1230, 2014.

[7] R. Ornelas-Kobayashi, A. Gogeascoechea and M. Sartori, "Person-Specific Biophysical Modeling of Alpha-Motoneuron Pools Driven by in vivo Decoded Neural Synaptic Input," *IEEE transactions on neural systems and rehabilitation engineering,* vol. 31, pp. 1532-1541, 2023.

[8] N. A. Maffiuletti, P. Aagaard, A. J. Blazevich, J. Folland, N. Tillin and J. Duchateau, "Rate

of force development: physiological and methodological considerations," *European journal of applied physiology,* vol. 116, pp. 1091-1116, 2016.

[9] J. Duchateau, J. G. Semmler and R. M. Enoka, "Training adaptations in the behavior of human motor units," *Journal of applied physiology,* vol. 101, no. 6, pp. 1766-1775, 2006.

[10] C. S. Sherrington, "Remarks on some aspects of reflex inhibition," *Proceedings of the Royal Society of London. Series B, Containing Papers of a Biological Character,* vol. 97, no. 686, pp. 519-545, 1925.

[11] N. Stifani, "Motor neurons and the generation of spinal motor neuron diversity," *Frontiers in cellular neuroscience,* vol. 8, p. 293, 2014.

[12] P. E. Ludwig, V. Reddy and M. Varacallo, "Neuroanatomy, neurons," 2017.

[13] M. J. van Putten, Dynamics of Neural Networks, Berlin, Heidelberg: Springer, 2020.

[14] B. P. Bean, "The action potential in mammalian central neurons," *Nature Reviews Neuroscience,* vol. 8, no. 6, pp. 451-465, 2007.

[15] W. A. Catterall, "The molecular basis of neuronal excitability," *Science,* vol. 223, no. 4637, pp. 653-661, 1984.

[16] K. C. Kanning, A. Kaplan and C. E. Henderson, "Motor neuron diversity in development and disease," *Annual review of neuroscience,* vol. 33, pp. 409-440, 2010.

[17] R. E. Burke, E. Jankowska and G. Ten Bruggencate, "A comparison of peripheral and rubrospinal synaptic input to slow and fast twitch motor units of triceps surae," *The Journal of physiology,* vol. 207, no. 3, pp. 709-732, 1970.

[18] E. R. Kandel, J. H. Schwartz, T. M. Jessell, S. Siegelbaum, A. J. Hudspeth and S. Mack, in *Principles of neural science*, New York, McGrawn-hill, 2000.

[19] E. Henneman, "Relation between size of neurons and their susceptibility to discharge," *Science,* vol. 126, no. 3287, pp. 1345-1347, 1957.

[20] A. J. Fuglevand, R. A. Lester and R. K. Johns, "Distinguishing intrinsic from extrinsic factors underlying firing rate saturation in human motor units," *Journal of neurophysiology,* vol. 113, no. 5, pp. 1310-1322, 2015.

[21] A. L. Revill and A. J. Fuglevand, "Inhibition linearizes firing rate responses in human motor units: implications for the role of persistent inward currents," *The Journal of physiology,* vol. 595, no. 1, pp. 179-191, 2017.

[22] C. J. Heckman, M. Johnson, C. Mottram and J. Schuster, "Persistent inward currents in spinal motoneurons and their influence on human motoneuron firing patterns," *The Neuroscientist,* vol. 14, no. 3, pp. 264-275, 2008.

[23] L. B. Orssatto, K. Mackay, A. J. Shield, R. L. Sakugawa, A. J. Blazevich and G. S. Trajano, "Estimates of persistent inward currents increase with the level of voluntary drive in low-threshold motor units of plantar flexor muscles," *Journal of neurophysiology,* vol. 125, no. 5, pp. 1746-1754, 2021.

[24] A. M. Zero, E. A. Kirk, K. Hali and C. L. Rice, "Firing rate trajectories of human motor units during isometric ramp contractions to 10, 25 and 50% of maximal voluntary contraction," *Neuroscience Letters,* vol. 762, p. 136118, 2021.

[25] A. Del Vecchio, D. Falla, F. Felici and D. Farina, "The relative strength of common synaptic input to motor neurons is not a determinant of the maximal rate of force development in humans," *Journal of Applied Physiology,* vol. 127, no. 1, pp. 205-214, 2019.

[26] K. S. Hong, N. Aziz and U. Ghafoor, "Motor-commands decoding using peripheral nerve signals: a review," *Journal of Neural Engineering,* vol. 15, no. 3, p. 031004, 2018.

[27] J. A. Gallego, T. R. Makin and S. D. McDougle, "Going beyond primary motor cortex to improve brain–computer interfaces," *Trends in neurosciences,* 2022.

[28] R. N. Lemon, "Descending pathways in motor control," *Annu. Rev. Neurosci,* vol. 31, pp. 195-218, 2008.

[29] A. B. Schwartz, "Movement: how the brain communicates with the world," *Cell,* vol. 164, no. 6, pp. 1122-1135, 2016.

[30] S. Virameteekul and R. Bhidayasiri, "We Move or Are We Moved? Unpicking the Origins of Voluntary Movements to Better Understand Semivoluntary Movements," *Frontiers in Neurology,* vol. 13, p. 187, 2022.

[31] J. C. Tuthill and E. Azim, "Proprioception," *Current Biology,* vol. 28, no. 5, pp. R194-R203, 2018.

[32] D. Farina and F. Negro, "Common synaptic input to motor neurons, motor unit synchronization, and force control," *Exercise and sport sciences reviews,* vol. 43, no. 1, pp. 23-33, 2015.

[33] C. J. Heckman and R. M. Enoka, "Physiology of the motor neuron and the motor unit," *Handbook of clinical neurophysiology,* vol. 4, no. Elsevier, pp. 119-147, 2004.

[34] D. Farina, F. Negro and J. L. Dideriksen, "The effective neural drive to muscles is the common synaptic input to motor neurons," *The Journal of physiology,* vol. 592, no. 16, pp. 3427-3441, 2014.

[35] R. R. Cisi and A. F. Kohn, "Simulation system of spinal cord motor nuclei and associated nerves and muscles, in a Web-based architecture," *Journal of computational neuroscience,* vol. 25, pp. 520-542, 2008.

[36] A. L. Hodgkin and A. F. Huxley, "A quantitative description of membrane current and its application to conduction and excitation in nerve," *The Journal of physiology,* vol. 117, no. 4, p. 500, 1952.

[37] F. Ponulak and A. Kasinski, "Introduction to spiking neural networks: Information processing, learning and applications," *Acta neurobiologiae experimentalis,* vol. 71, no. 4, pp. 409-433, 2011.

[38] C. D. Schuman, T. E. Potok, R. M. Patton, J. D. Birdwell, M. E. Dean, G. S. Rose and J. S. Plank, "A survey of neuromorphic computing and neural networks in hardware," *arXiv preprint,* p. arXiv:1705.06963, 2017.

[39] A. Destexhe, "Conductance-based integrate-and-fire models," *Neural Computation,* vol. 9, no. 3, pp. 503-514, 1997.

[40] T. Oya, S. Riek and A. G. Cresswell, "Recruitment and rate coding organisation for soleus motor units across entire range of voluntary isometric plantar flexions," *The Journal of physiology,* vol. 587, no. 19, pp. 4737-4748, 2009.

[41] J. Duchateau and R. M. Enoka, "Distribution of motor unit properties across human muscles," *Journal of Applied Physiology,* vol. 132, no. 1, pp. 1-13, 2022.

[42] M. V. Cutsem, P. Feiereisen, J. Duchateau and K. Hainaut, "Mechanical properties and behaviour of motor units in the tibialis anterior during voluntary contractions," *Canadian journal of applied physiology,* vol. 22, no. 6, pp. 585-597, 1997.

[43] J. Duchateau and K. Hainaut, "Effects of immobilization on contractile properties, recruitment and firing rates of human motor units," *The Journal of physiology,* vol. 422, no. 1, pp. 55-65, 1990.

[44] R. M. Enoka and J. Duchateau, "Rate coding and the control of muscle force," *Cold Spring Harbor perspectives in medicine,* vol. 7, no. 10, p. a029702, 2017.

[45] H. S. Milner-Brown, R. B. Stein and R. Yemm, "The contractile properties of human motor units during voluntary isometric contractions," *The Journal of physiology,* vol. 228, no. 2, pp. 285-306, 1973.

[46] J. E. Desmedt and E. Godaux, "Ballistic contractions in man: characteristic recruitment pattern of single motor units of the tibialis anterior muscle," *The Journal of physiology,* vol. 264, no. 3, pp. 673-693, 1977.

[47] J. D. Miller, C. J. Lund, M. D. Gingrich, K. L. Schtul, M. E. Wray and T. J. Herda, "The effect of rate of torque development on motor unit recruitment and firing rates during isometric voluntary trapezoidal contractions," *Experimental Brain Research,* vol. 237, pp. 2653-2664, 2019.

[48] A. Holobar, M. A. Minetto and D. Farina, "Accurate identification of motor unit discharge patterns from high-density surface EMG and validation with a novel signal-based performance metric," *Journal of neural engineering,* vol. 11, no. 1, p. 016008, 2014.

[49] D. Farina, A. Holobar, R. Merletti and R. M. Enoka, "Decoding the neural drive to muscles from the surface electromyogram," *Clinical neurophysiology,* vol. 121, no. 10, pp. 1616-1623, 2010.

[50] S. H. Nawab, S. S. Chang and C. J. De Luca, "High-yield decomposition of surface EMG signals," *Clinical neurophysiology,* vol. 121, no. 10, pp. 1602-1615, 2010.

[51] C. Dai and X. Hu, "Independent component analysis based algorithms for high-density electromyogram decomposition: Systematic evaluation through simulation," *Computers in biology and medicine,* vol. 109, pp. 171-181, 2019.

[52] A. Holobar and D. Zazula, "Multichannel blind source separation using convolution kernel compensation," *EEE Transactions on Signal Processing,* vol. 55, no. 9, pp. 4487-4496, 2007.

[53] J. H. Block, J. P. Van Dijk, G. Drost, M. J. Zwarts and D. F. Stegeman, "A high-density multichannel surface electromyography system for the characterization of single motor units," *Review of scientific instruments,* vol. 73, no. 4, pp. 1887-1897, 2002.

[54] P. Aagaard, J. Bojsen-Møller and J. Lundbye-Jensen, "Assessment of neuroplasticity with strength training," *Exercise and Sport Sciences Reviews,* vol. 48, no. 4, pp. 151-162, 2020.

[55] Z. H. Liu, P. K. Yip, L. Adams, M. Davies, J. W. Lee, G. J. Michael and A. T. Michael-Titus, " A single bolus of docosahexaenoic acid promotes neuroplastic changes in the innervation of spinal cord interneurons and motor neurons and improves functional recovery after spinal cord injury," *Journal of Neuroscience,* vol. 35, no. 37, pp. 12733-12752, 2015.

[56] H. J. Chen, J. Tani, C. S. Lin, T. S. Chang, Y. C. Lin, T. W. Hsu and J. Y. Sung,

"Neuroplasticity of peripheral axonal properties after ischemic stroke," *Plos one,* vol. 17, no. 10, p. e0275450, 2022.

[57] T. H. Hutson and S. Di Giovanni, "The translational landscape in spinal cord injury: focus on neuroplasticity and regeneration," *Nature Reviews Neurology,* vol. 15, no. 12, pp. 732-745, 2019.

[58] M. Puderbaugh and P. D. Emmady, "Neuroplasticity. In StatPearls [Internet]," *StatPearls Publishing,* 2023.

[59] G. Uswatte and E. Taub, "Constraint-induced movement therapy: a method for harnessing neuroplasticity to treat motor disorders," *Progress in brain research,* vol. 207, pp. 379-401, 2013.

[60] C. Patten and G. Kamen, "Adaptations in motor unit discharge activity with force control training in young and older human adults," *European journal of applied physiology,* vol. 83, pp. 128-143, 2000.

[61] J. L. Stephenson and K. S. Maluf, "Dependence of the paired motor unit analysis on motor unit discharge characteristics in the human tibialis anterior muscle," *Journal of neuroscience methods,* vol. 198, no. 1, pp. 84-92, 2011.

[62] A. Adam and C. J. De Luca, "Firing rates of motor units in human vastus lateralis muscle during fatiguing isometric contractions," *Journal of Applied Physiology,* vol. 99, no. 1, pp. 268-280, 2005.

[63] L. Mesin, E. Merlo, R. Merletti and C. Orizio, "Investigation of motor unit recruitment during stimulated contractions of tibialis anterior muscle," *Journal of Electromyography and Kinesiology,* vol. 20, no. 4, pp. 580-589, 2010.

[64] A. Del Vecchio, "Neuromechanics of The Rate of Force Development," *Exercise and Sport Sciences Reviews,* vol. 51, no. 1, pp. 34-42, 2023.

[65] J. P. Gabriel, J. Ausborn, K. Ampatzis, R. Mahmood, E. Eklof-Ljunggren and A. El Manira, "Principles governing recruitment of motoneurons during swimming in zebrafish," *Nature neuroscience,* vol. 14, no. 1, pp. 93-99, 2011.

[66] B. Morel, D. M. Rouffet, D. Saboul, S. Rota, M. Clémençon and C. A. Hautier, "Peak torque and rate of torque development influence on repeated maximal exercise performance: contractile and neural contributions," *PLoS One,* vol. 10, no. 4, p. e0119719, 2015.

[67] A. Del Vecchio, F. Negro, D. Falla, I. Bazzucchi, D. Farina and F. Felici, "Higher muscle fiber conduction velocity and early rate of torque development in chronically strength-trained individuals," *Journal of applied physiology,* vol. 125, no. 4, pp. 1218-1226, 2018.

[68] A. Del Vecchio, F. Negro, A. Holobar, A. Casolo, J. P. Folland, F. Felici and D. Farina, "You are as fast as your motor neurons: speed of recruitment and maximal discharge of motor neurons determine the maximal rate of force development in humans," *The Journal of physiology,* vol. 597, no. 9, pp. 2445-2456, 2019.

[69] C. J. Heckman, C. Mottram, K. Quinlan, R. Theiss and J. Schuster, "Motoneuron excitability: The importance of neuromodulatory inputs," *Clinical Neurophysiology,* vol. 120, no. 12, pp. 2040-2054, 2009.

[70] I. Y. Kuo and B. E. Ehrlich, "Signaling in muscle contraction," *Cold Spring Harbor perspectives in biology,* vol. 7, no. 2, p. a006023, 2015.

[71] A. J. Fuglevand, D. A. Winter and A. E. Patla, "Models of recruitment and rate coding organization in motor-unit pools," *Journal of neurophysiology,* vol. 70, no. 6, pp. 2470-2488, 1993.

[72] C. J. De Luca and P. Contessa, "Hierarchical control of motor units in voluntary contractions," *Journal of neurophysiology,* vol. 107, no. 1, pp. 178-195, 2012.

[73] C. J. De Luca and E. C. Hostage, "Relationship between firing rate and recruitment threshold of motoneurons in voluntary isometric contractions," *Journal of neurophysiology,* vol. 104, no. 2, pp. 1034-1046, 2010.

[74] C. J. Heckman and R. M. Enoka, "Motor unit," *Comprehensive physiology,* no. 4, pp. 2629-2682, 2012.

[75] J. E. Desmedt and E. Godaux, "Fast motor units are not preferentially activated in rapid voluntary contractions in man," *Nature,* vol. 267, no. 5613, pp. 717-719, 1997.

[76] A. Gogeascoechea, A. Kuck, E. Van Asseldonk, F. Negro, J. R. Buitenweg, U. S. Yavuz and M. Sartori, "Interfacing with alpha motor neurons in spinal cord injury patients receiving trans-spinal electrical stimulation," *Frontiers in neurology,* vol. 11, p. 493, 2020.

[77] A. Del Vecchio, A. Ubeda, M. Sartori, J. M. Azorin, F. Felici and D. Farina, "Central nervous system modulates the neuromechanical delay in a broad range for the control of muscle force," *Journal of applied physiology,* vol. 125, no. 5, pp. 1404-1410, 2018.

[78] M. Kristan, A. Leonardis and D. Skočaj, "Multivariate online kernel density estimation with Gaussian kernels," *Pattern recognition,* vol. 44, no. 10-11, pp. 2630-2642, 2011.

[79] C. K. Thomas, B. Bigland-Richie and R. S. Johansson, "Force-frequency relationships of human thenar motor units," *Journal of neurophysiology,* vol. 65, no. 6, pp. 1509-1516, 1991.

[80] V. G. Macefield, A. J. Fuglevand and B. R. Bigland-Ritchie, "Contractile properties of single motor units in human toe extensors assessed by intraneural motor axon stimulation," *Journal of neurophysiology,* vol. 75, no. 6, pp. 2509-2519, 1996.

[81] Y. Masakado, K. Akaboshi, M. A. Nagata, A. Kimura and N. Chino, "Motor unit firing behavior in slow and fast contractions of the first dorsal interosseous muscle of healthy men," *Electroencephalography and Clinical Neurophysiology/Electromyography and Motor Control,* vol. 97, no. 6, pp. 290-295, 1995.

[82] J. E. Davis, "Combining error ellipses," *CXC memo,* 2007.

[83] C. Roussel, T. Erneux, S. N. Schiffmann and D. Gall, "Modulation of neuronal excitability by intracellular calcium buffering: from spiking to bursting," *Cell Calcium,* vol. 39, no. 5, pp. 455-466, 2006.

[84] R. Vastano and M. A. Perez, "Changes in motoneuron excitability during voluntary muscle activity in humans with spinal cord injury," *Journal of neurophysiology,* vol. 123, no. 2, pp. 454-461, 2020.

[85] L. J. Volz, M. Hamada, J. C. Rothwell and C. Grefkes, "What makes the muscle twitch: motor system connectivity and TMS-induced activity," *Cerebral Cortex,* vol. 25, no. 9, pp. 2346-2353, 2015.

[86] L. Macpherson and D. R. Wilkie, "The duration of the active state in a muscle twitch," *The Journal of Physiology,* vol. 124, no. 2, p. 292, 1954.

[87] J. Nijssen, L. H. Comley and E. Hedlund, "Motor neuron vulnerability and resistance in amyotrophic lateral sclerosis," *Acta neuropathologica,* vol. 133, pp. 863-885, 2017.

# Appendix

## A.1. MN pool models driven by $\Delta IF_{20}$

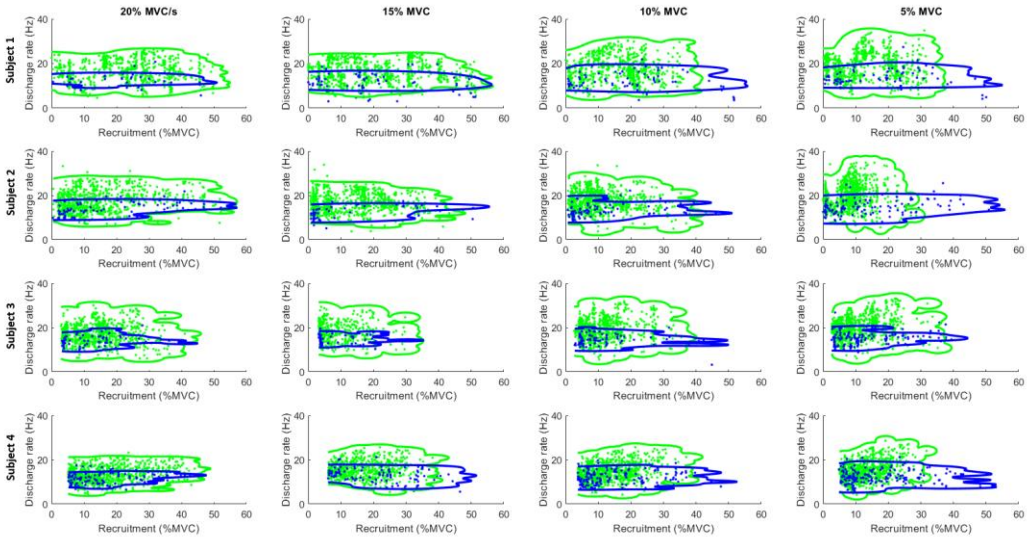


*A 1. Firing dynamics analysis of the four subjects and multiple RFDs (5, 10, 15, and 20% MVC/s) between in vivo MNs (blue) vs in silico generated MN models (green) driven by $\Delta IF_{20}$ using the kernel density function method.*

## A.2. MN pool models driven by slope-specific $\Delta IF$

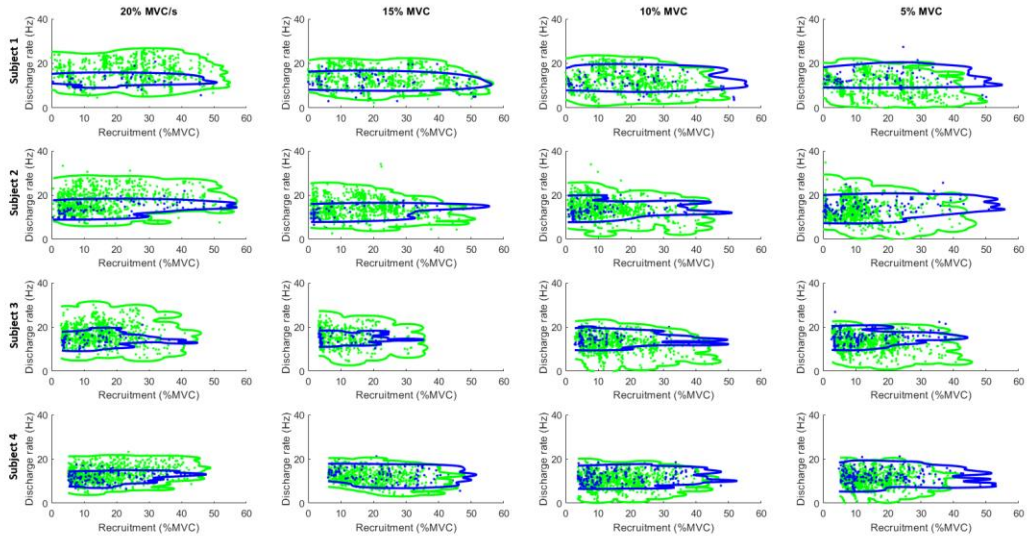


*A 2. Firing dynamics analysis of the four subjects and multiple RFDs (5, 10, 15, and 20% MVC/s) between in vivo MNs (blue) vs in silico generated MN models (green) driven by $\Delta IF$ specific for each RFD using the kernel density function method.*

## A.3. Subject 1 firing dynamics

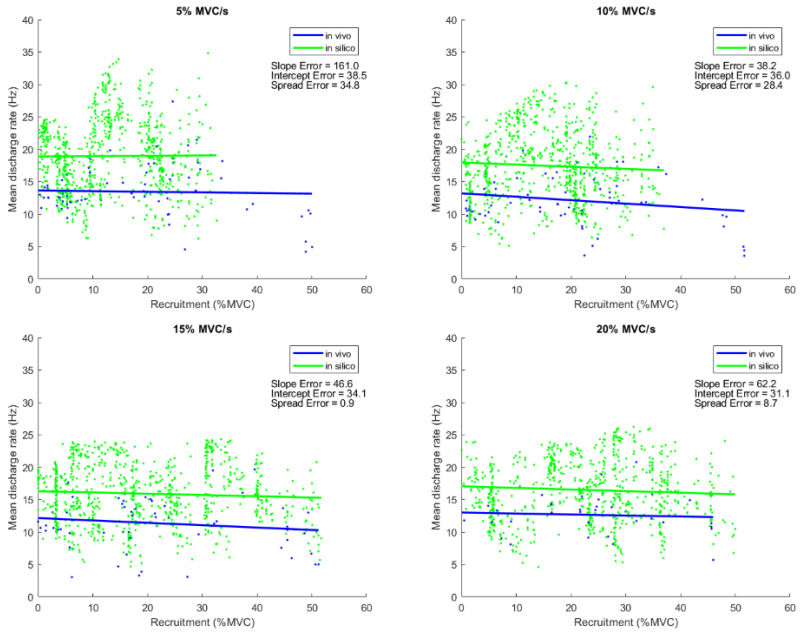


*A 3. Firing dynamics analysis for subject 1. The relative error estimation of the firing activity at multiple RFDs (5, 10, 15, and 20% MVC/s) between in vivo MNs (blue) vs in silico generated MN models (green) driven by $\Delta IF_{20}$ using the linear model method. With this method three cost functions are estimated: Slope error, intercept error, and spread error.*

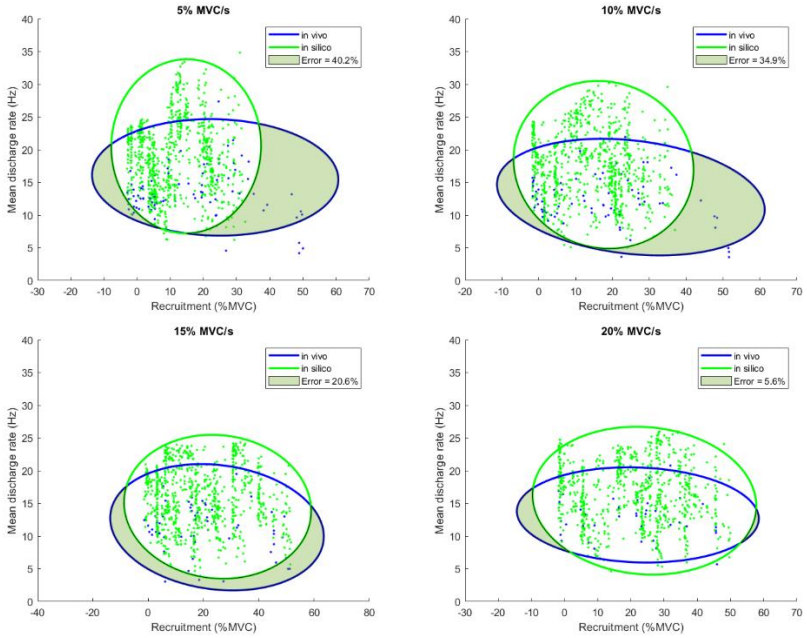


*A 4. Firing dynamics analysis for subject 1. The relative error estimation of the firing activity at multiple RFDs (5, 10, 15, and 20% MVC/s) between in vivo MNs (blue) vs in silico generated MN models (green) driven by $\Delta IF_{20}$ using the covariance matrix-based ellipse method. This method estimates only one cost function: the difference between the areas of the computed ellipses.*

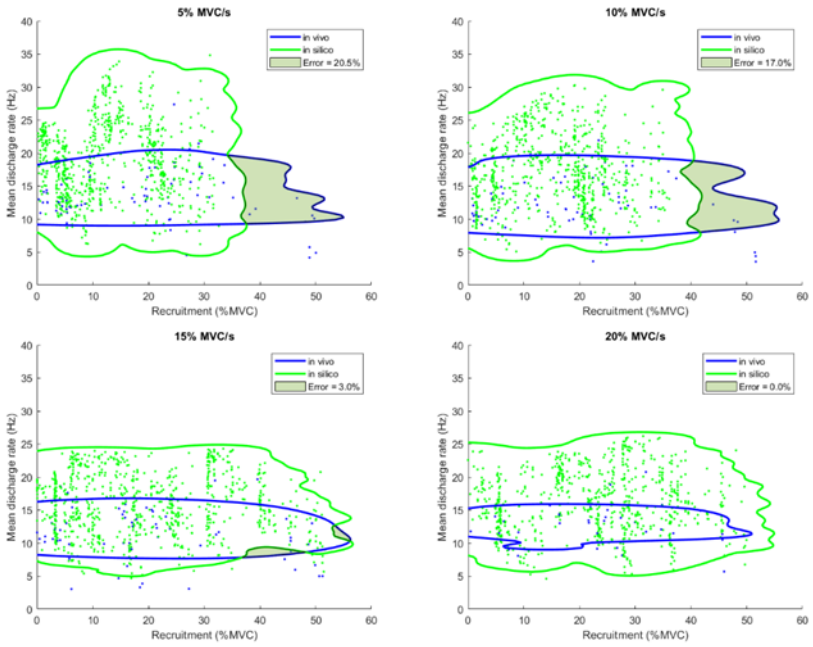


*A 5. Firing dynamics analysis for subject 1. The relative error estimation of the firing activity at multiple RFDs (5, 10, 15, and 20% MVC/s) between in vivo MNs (blue) vs in silico generated MN models (green) driven by $\Delta IF_{20}$ using the kernel density function method. This method estimates only one cost function: the difference between the areas of the kernel density functions.*

## A.4. Subject 2 firing dynamics

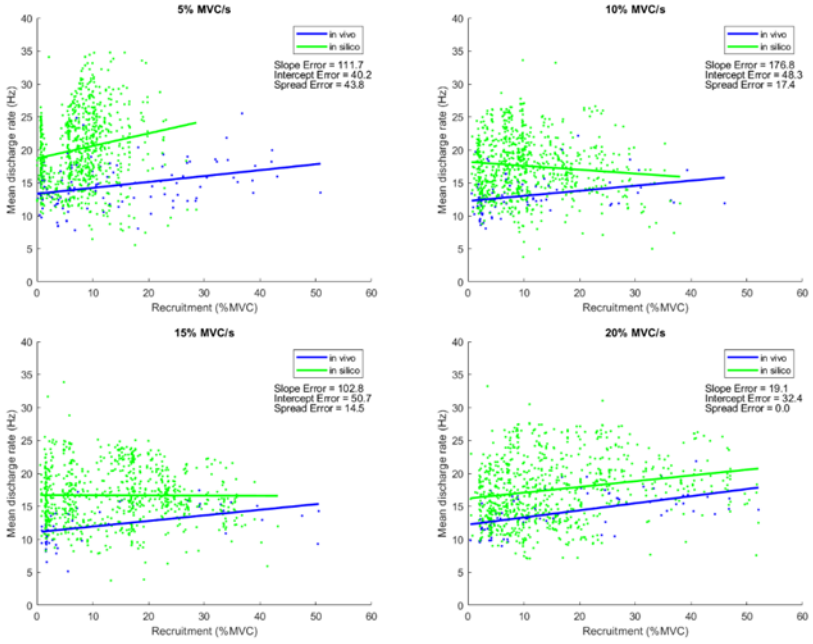


*A 6. Firing dynamics analysis for subject 2. The relative error estimation of the firing activity at multiple RFDs (5, 10, 15, and 20% MVC/s) between in vivo MNs (blue) vs in silico generated MN models (green) driven by $\Delta IF_{20}$ using the linear model method. With this method three cost functions are estimated: Slope error, intercept error, and spread error.*

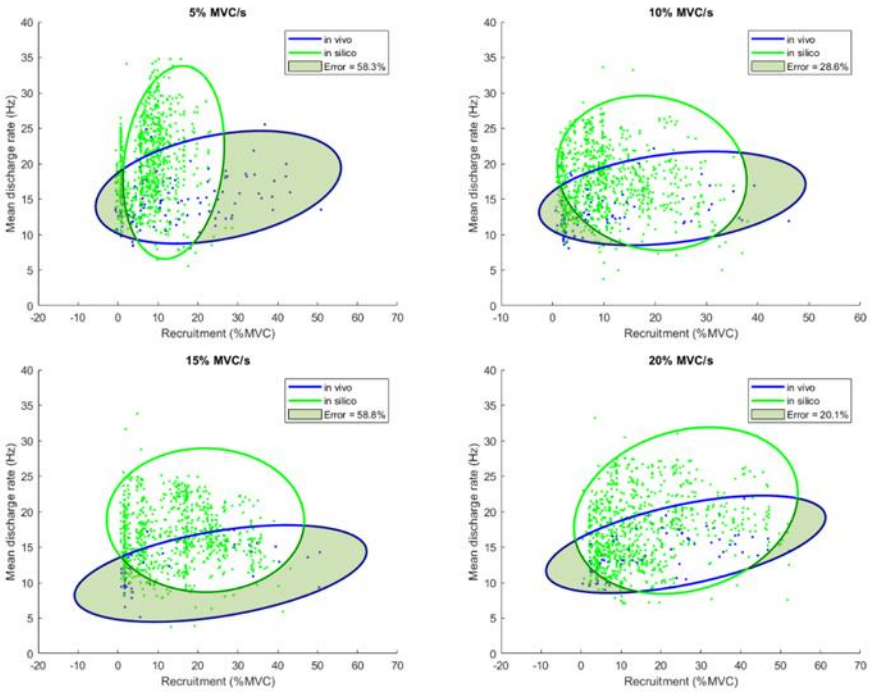


*A 7. Firing dynamics analysis for subject 2. The relative error estimation of the firing activity at multiple RFDs (5, 10, 15, and 20% MVC/s) between in vivo MNs (blue) vs in silico generated MN models (green) driven by $\Delta IF_{20}$ using the covariance matrix-based ellipse method. This method estimates only one cost function: the difference between the areas of the computed ellipses.*

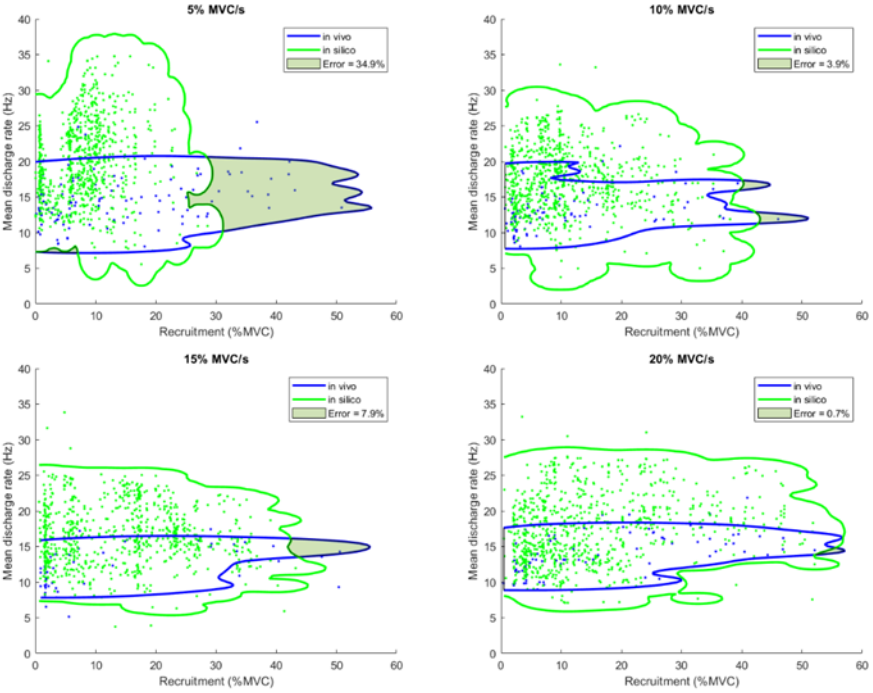


*A 8. Firing dynamics analysis for subject 2. The relative error estimation of the firing activity at multiple RFDs (5, 10, 15, and 20% MVC/s) between in vivo MNs (blue) vs in silico generated MN models (green) driven by $\Delta IF_{20}$ using the kernel density function method. This method estimates only one cost function: the difference between the areas of the kernel density functions.*

## A.5. Subject 3 firing dynamics

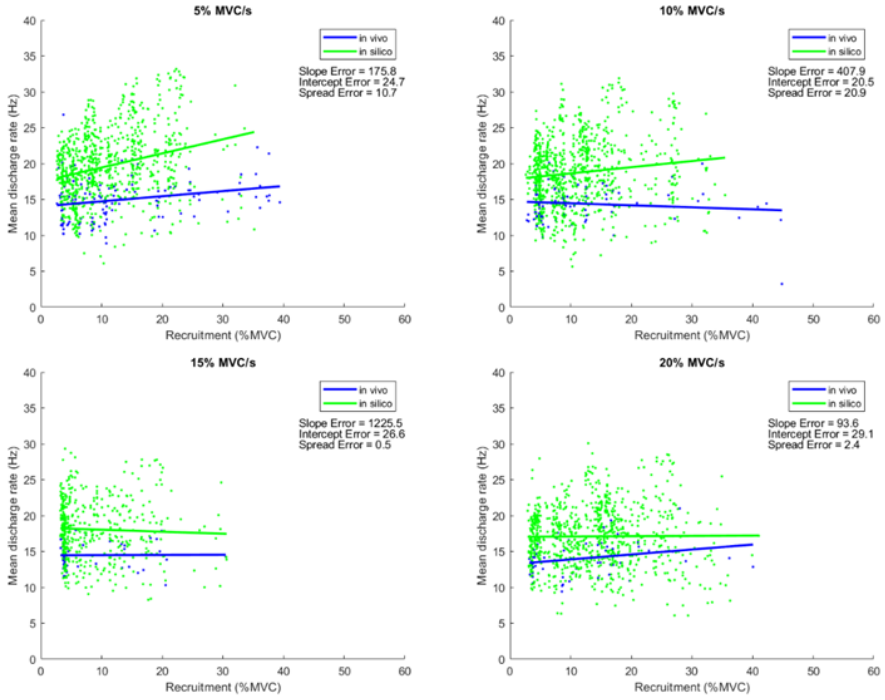


*A 9. Firing dynamics analysis for subject 3. The relative error estimation of the firing activity at multiple RFDs (5, 10, 15, and 20% MVC/s) between in vivo MNs (blue) vs in silico generated MN models (green) driven by $\Delta IF_{20}$ using the linear model method. With this method three cost functions are estimated: Slope error, intercept error, and spread error.*

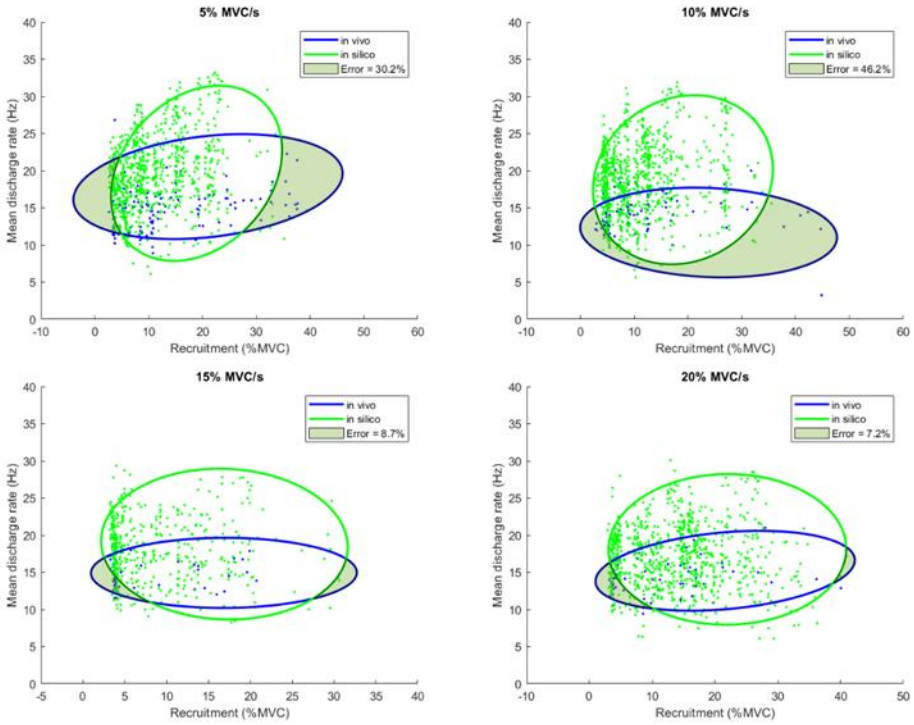


*A 10. Firing dynamics analysis for subject 3. The relative error estimation of the firing activity at multiple RFDs (5, 10, 15, and 20% MVC/s) between in vivo MNs (blue) vs in silico generated MN models (green) driven by $\Delta IF_{20}$ using the covariance matrix-based ellipse method. This method estimates only one cost function: the difference between the areas of the computed ellipses.*

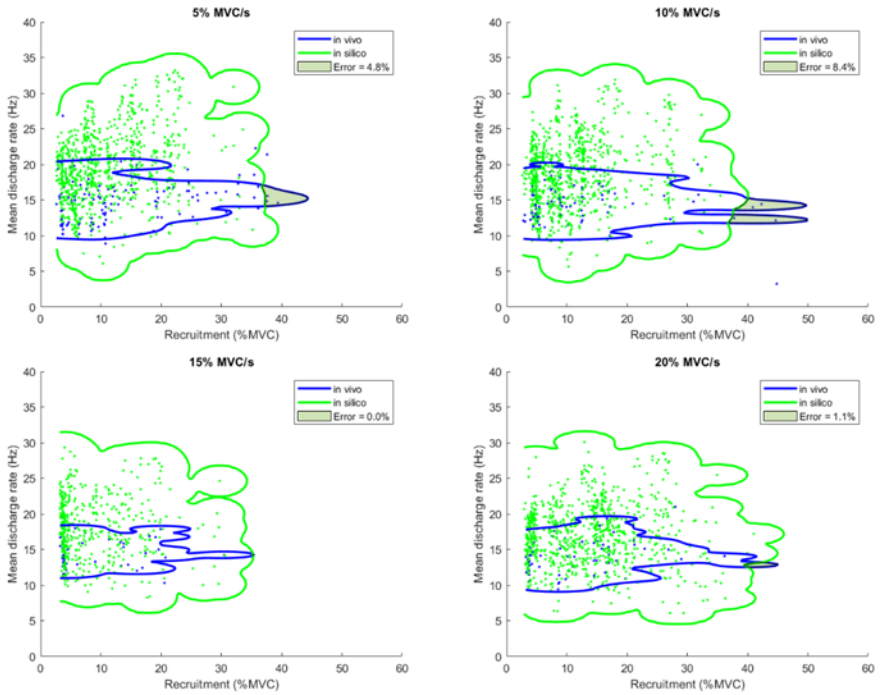


*A 11. Firing dynamics analysis for subject 3. The relative error estimation of the firing activity at multiple RFDs (5, 10, 15, and 20% MVC/s) between in vivo MNs (blue) vs in silico generated MN models (green) driven by $\Delta IF_{20}$ using the kernel density function method. This method estimates only one cost function: the difference between the areas of the kernel density functions.*